Efficient Photocatalytic and EMI Shielding Properties of CdO/ La2O3 Nanocomposites

Senthil S (ssenthil_14@yahoo.co.in)
Presidency College https://orcid.org/0000-0003-0079-8174
SRINIVASAN S
Presidency College
THANGEESWARI T
Vel Tech High Tech Dr Rangarajan Dr Sakunthala Engineering College Department of Science and Humanities: Vel Tech High Tech Dr Rangarajan Dr Sakunthala Engineering College
MADHU B J
Government Science College Chitradurga
SILAMBARASAN M
PRIST University

Research Article

Keywords: Dielectric, EMI shielding, CIE colour coordinates, polymer nanocomposite, rare earth element

Posted Date: March 30th, 2021

DOI: https://doi.org/10.21203/rs.3.rs-341051/v1

Efficient Photocatalytic and EMI shielding properties of CdO/ La_2O_3 nanocomposites

Senthil. S[1,2*], Srinivasan. S[2], Thangeeswari. T[3], Madhu. B.J[4], and Silambarasan. M[5]

[1]Department of Physics, St.Peters College of Engineering and Technology, Chennai-600 054, Tamilnadu, India

[2]Department of Physics, Presidency College, University of Madras, Chennai-600005, Tamilnadu, India

[3]Department of Physics, Vel Tech Multitech Dr.Rangarajan Dr.Sakunthala Engineering College, Chennai-600 062, Tamilnadu, India

[4]Department of Physics, Government Science College, Chitradurga, Karnataka- 577501, India

[5]Department of Physics, PRIST University, Puducherry-605007, India

Abstract

The pure CdO and CdO/La_2O_3, and CdO/La_2O_3/PVP nanocomposites were synthesized by microwave irradiation method. The prepared samples are analyzed by X-Ray diffraction (XRD), Fourier Transform infrared spectroscopy (FT-IR), Scanning electron microscope (SEM), Transmission electron microscope (TEM), UV visible spectrometer, Photoluminescence (PL), and Vibrating sample magnetometer (VSM). XRD and FTIR studies confirmed the formation of binary metallic nanocomposites. SEM and TEM analysis authenticate that the addition of lanthanum oxide and PVP influences the size and morphology of CdO nanoparticles the bandgap value can be tuned by the addition of La_2O_3 and PVP. Photoluminescence spectra show the violet emission in the region between 432 nm to 460 nm and the green emission peak at 529 nm for all three synthesized samples. CIE color coordinates for CdO and CdO/La_2O_3, and CdO/La_2O_3/PVP nanocomposites were also estimated from emission spectrum. The VSM results confirmed that the nanocomposites possess the weak ferromagnetic properties due to the inclusion of La_2O_3 and PVP. The dielectric constant, electrical conductivity and dielectric loss values at room temperature have been analyzed for CdO and CdO/La_2O_3, and CdO/La_2O_3/PVP nanocomposites. Among the three synthesized samples, the CdO/La_2O_3/PVP nanocomposite attain high electromagnetic shielding efficiency. Furthermore, the rare earth element lanthanum oxide and PVP enhances the efficiency of photocatalytic degradation of MB dye.

Keywords: Dielectric, EMI shielding, CIE colour coordinates, polymer nanocomposite, rare earth element

[*] *Corresponding Author:*
Address to Correspondence:
Senthil. S
Research Scholar
Department of Physics
Presidency College,
Chennai-600 005, Tamil nadu, India
9677177293,
e.mail: ssenthil_14@yahoo.co.in

1. Introduction

In recent research, the Cadmium Oxide (CdO) transparent conducting oxides (TCOs) are received more attention towards optoelectronic devices. Due to its unique properties such as good optical transmittance and high electrical conductivity, CdO is used in various practical applications such as solar cells, sensors, light emitting dodes (LED), optical waveguides and flat panel displays [1,2]. Cadmium Oxide (CdO) is an n-type semiconductor with low resistivity, more carrier mobility and high optical transmittance in visible and near IR regions. CdO possesses face-centered cubic structure with enhanced mechanical property and chemical stability [2-4]. The significant analysis of the electronic properties of CdO nanoparticles makes which can be used in specified optoelectronic applications. In general, the electronic properties of nanoparticles depends on various factors such as doping element, dopant concentration, Temperature, surface to volume ratio and quantum confinement effect [2,5-7].

Nanocomposites are the new materials with suitable combination of the semiconductor metal oxides. This combined metal oxide shows the advanced peculiar property by the process of interaction between either metal- metal interactions or metal-oxygen-metal interactions [8]. In recent research field, it is a challenging work to develop the new nanocomposites with enhanced magnetic, optoelectronic and physic-chemical properties such as by integrating different metal oxides [9, 10]. Sahu et al observed that the combination of ZnO and CdO increases the properties of both ZnO and CdO [11]. Castro et al confirms that the efficiency of the solar cell is enriched by creating defect related optical absorption in CdO:ZnO nanocomposites [12]. The gas sensing properties of ZnO: TiO2-based nanocomposites were enhanced by adding another metal oxide CdO [13]. Wang et al proves that the AgO: La_2O_3 nanocomposites proceed as good antibacterial agent [14]. Similarly, combination of cadmium oxide and zinc oxide nanocomposites act as a good catalysis in removal of industrial pollutant in water treatment [15]. Sivaram et al studies on electrochemical confirms that the addition of ZnO in PbO nanoparticles enhances the electro chemical properties [16].

Among the various semiconductor metal oxides, the rare earth metal oxides are gifted elements due to their unique properties such as optical, magnetic and electrical properties [17]. Rare earth elements show the special spectral configurations with partially shielded 4f-4f electron transition [18, 19]. Recent research trends move towards the usage of rare earth element, lanthanum oxide in various applications like superconductor, fiber optics, sensors, gas convector in automobiles, light emitting phosphors and laser [20, 21]. Uma et al. observed that the lanthanum oxide deposition layer between Au and GaN semiconductor enhanced the dielectric properties by metal insulator-semiconductor combination [17].

In present electronic world, in all electronic appliances the Electromagnetic Interference (EMI) phenomenon reduces the performances of the electronic devices. To overcome the EMI shielding is required which is attained by using flexible and light weight nanocomposites. To increase the shielding efficiency (SE), the material should possess the unique properties like stable, enhanced

permittivity, electrical conductivity and magnetic dipoles. The high shielding efficiency is achieved by use the nanomaterials with more surface to volume ratio, defects and charge carrier mobility [22, 23]. In carbon nanotubes, the EMI shielding is attained by both electromagnetic absorption and reflection process due to free electrons. Advanced research in nanocomposites confirms that the carbon nanotubes with polylactic acid nanocomposites in 3-dimentional ink form produce more EMI SE than the nanocomposites in solid form [24]. Furthermore, the incorporation of polymer such as polyaniline (PANI), hexagonal boron nitride (HBN) and Polyvinylpyrrolidone (PVP) with nanocomposites enriches the optical, electronic, dielectric, magnetic, EMI SE, mechanical properties and thermal stability [25, 26].

The dielectric measurements are used to analyze relaxation and conductivity process in materials. The parameters such as particle size, large surface to volume ratio, defects, temperature, doping and plays a vital role in dielectric property in nanoparticles [27-29]. Zhao et al results observed that the increase in doping amount of lanthanum oxide with BaSrTiO3 ceramics increases the dielectric constant [30]. Ebrahimzadeh et al results confirmed that the aluminum and tin doped

lanthanum oxide nanocomposites possess the high dielectric constant [31]. On the other side, the addition capping agent into nanoparticles also increases the dielectric constant via interfacial polarization process [32].

This research work is to enrich the electronic, electrical, photocatalytic and magnetic properties of CdO nanoparticles by applying heterogeneous system of CdO/La_2O_3/PVP. The effect of rare earth element lanthanum oxide and capping agent PVP on the electronic, electrical, photocatalytic activity and magnetic properties of CdO is analyzed and reported.

2. Experimental Details

2.1. Material synthesis

The samples were synthesized by microwave irradiation method. The advantage of microwave irradiation method is high reaction rate, simple to handle, economically low, low time spending and produces the highly pure uniform nanoparticles [33]. The cadmium nitrate tetra hydrate (Cd $(NO_3)_2 \cdot 4H_2O$) and lanthanum III nitrate hexahydrate (LaN_3O_9) were employed as metal precursors and for capping agent polyvinylpyrrolidone (PVP) is used. Both CdO and La_2O_3 are having different structure. The concentrations of 90% CdO and 10% La_2O_3 were dissolved in de ionized water and then ammonia solution is added to precursors under stirring for 8h. The resulting precipitate was washed with distilled water and acetone again and again to remove the impurities. The obtained precipitate was placed in microwave oven for 20 minutes. Finally the product was calcined at 300°C for 4hr in muffle furnace to get CdO/La_2O_3 nanocomposite. Similarly the capping agent polyvinylpyrrolidone (PVP 10%) mixed with CdO/La_2O_3 (0.9: 0.1) and synthesized by the same above mentioned procedure. To compare the properties, the pure CdO nanoparticle also synthesized.

2.2 Characterization Techniques

The crystalline nature was studied by X-ray diffraction using Cu Kα radiation (λ=1.5406Å) with the scanning rate of $0.05°s^{-1}$ in the 2θ range from 20° to 80°. Micro structure and morphology of the prepared pure CdO, CdO/La_2O_3, and CdO/La_2O_3/PVP nanocomposite were investigated by Scanning Electron Microscopy (SEM, CAREL ZEISS, EVO 18 ~5 kV) and High Resolution Transmission Electron Microscopy (HR-TEM, FEI-TECNAI G2-20 ~200 kV) respectively. Photoluminescence (PL) spectra were recorded using a He-Cd laser source with an excitation wavelength of 325 nm by PERKIN ELMER L45 fluorescence spectrophotometer at room temperature. The molecular configuration of synthesized samples was studied by Shimadzu FT-IR 3000 with potassium bromide diluents. The band gap value and optical absorbance of the prepared nanocomposites were studied by using (Shimadzu UV-2450) UV-Vis-NIR spectrophotometer. The ferromagnetic possessions of the synthesized samples at room temperature were analyzed by using Vibrating Sample Magnetometer (Lakeshore VSM 7407). The dielectric ac conductivity and electromagnetic shielding studies performed by using impedance analyzer (model HIOKI 3532-50 LCR Hi Tester Version 2.3) over the frequency range 42Hz-5MHz).

2.3. Photocatalytic Experimental Arrangements

The photocatalytic activity of pure CdO, CdO/La_2O_3 and CdO/La_2O_3/PVP hybrid nanocomposite were deliberate by methylene blue (MB) degradation in aqueous solution under UV light irradiation. The experiment was performed by adding 5 mg of synthesized samples to 10 mg/L of MB in 50 ml beaker. Before irradiation, the mixture solution were stirred for 30 minutes and kept in a dark place to obtain adsorption-desorption equilibrium and the concentration of the solution was taken as initial concentration (C_o) of the dye solution. Then 5 ml of the solution was taken out from the mixture solution and the UV-vis spectra (Carry-5000) of the MB solution was examined every 30 min of intervals. The degradation percentage of dye is calculated from the following equation

$$\eta = \left[\frac{(Co - Ct)}{Co}\right] \times 100$$

-

where, η is the degradation percentage, C_o is the concentration of the dye (mg/L) at time 0 min and C_t is the concentration of the dye after irradiation in 30 min time interval.

3. Results and Discussions

3.1 Phase Analysis

The structural and phase analysis of the synthesized samples are carried out by diffraction patterns of XRD. Figure 1 shows the XRD patterns of pure CdO, CdO/La_2O_3, and CdO/La_2O_3/PVP nanocomposites. From XRD pattern, we can analyze the effect of lanthanum oxide and PVP addition on the CdO nanoparticles. The diffraction patterns in CdO/La_2O_3, and CdO/La_2O_3/PVP nanocomposites show the more peaks corresponds to pure CdO and few peaks corresponds to lanthanum oxide in nanocomposites [11]. This few additional peaks attributes to changes in crystalline structure of synthesized nanocomposites. The diffraction peaks at 2θ values of 33.04°, 38.4°, 55.24°, 66.11° and 69.46° are corresponds to (111), (200), (220), (311) and (222) planes of pure CdO nanoparticles respectively [1,2]. Similarly the peaks at 2θ values of 28.13°, 30.4° and 43.93° are associated with (002), (400), and (125) planes of La_2O_3 [17, 34]. All the obtained diffraction peaks are confirmed with JCPDS no 75-0592 (CdO) and 65-3185 (La_2O_3). In addition, we observed the peaks at 23.4° and 22.82° which corresponds to La_2O_3 in CdO/La_2O_3, and CdO/ La_2O_3/PVP nanocomposites (JCPDS no 84-1963) [35]. The observed diffraction peaks for both CdO and La_2O_3 confirms the cubical phase formation of both CdO and La_2O_3 nanocomposites. The sharp intense diffraction peaks in CdO/La_2O_3, and CdO/La_2O_3/PVP shows that the synthesized nanocomposites are in poly crystalline structure [36]. The calculated value of lattice constant 4.687A for synthesized CdO nanoparticles is matched with standard value (4.697A$^{\circ}$). The obtained lattice constant and unit cell volume of CdO/La_2O_3, and CdO/La_2O_3/PVP nanocomposites increases compare to pure CdO nanoparticles which confirms the incorporation of La_2O_3 and PVP into CdO lattice. This may be attributed to presence defects, impurity and strain in lattice [2]. In other words, reduction in particle size increases the surface area and there by increases the grain volume. The increases in grain volume allow more particle interactions at the interface. The more intense peak is employed to find the crystallite size using Debye Scherrer's equation

$$D = \frac{0.89\,\lambda}{\beta\cos\theta}$$

Where D is size of the crystallite particle, λ is the wavelength of incident X-ray, β is the full width at half maximum (FWHM) measured in radians and θ is the Bragg's angle of diffraction peak. The nanoparticle size of pure CdO, CdO/La_2O_3, and CdO/La_2O_3/PVP were found to be 31.3 nm, 23.7 nm, and 19.38 nm respectively.

3.2 Functional group Analysis by FTIR

Figure 2 shows the FTIR spectra of CdO, CdO/La_2O_3 and CdO/La_2O_3/PVP nanocomposites which confirms the presence of functional groups in binary systems. FTIR spectra were recorded in terms of wave number between 4000 - 400 cm^{-1}. The broad absorption peaks near 3445cm^{-1} is corresponds to OH stretching bond of water molecules due to moisture. The IR band near 1381 cm^{-1} for all three samples is assigned to C-O stretching vibration. The absorption band at 1628 cm^{-1} for pure CdO, 1311 cm-1 for CdO/La_2O_3 and 1583 cm^{-1} for CdO/La_2O_3/PVP is attributed to bending vibration band of physically adsorbed water molecules [21, 36-37]. The peaks at 2923 cm^{-1}, 2916 cm^{-1} & 2854 cm^{-1} in CdO, CdO/La_2O_3 and CdO/La_2O_3/PVP nanocomposites

is belongs to carbonyl group of O–C–O vibrations [38]. On other side, PVP in CdO increases the stability of CdO via carbonyl group [39]. Hence it is confirmed that the prepared sample is the combination of CdO, La_2O_3 and PVP.

3.3 Surface Morphology Analysis

Figure 3(a-c) represents the SEM images for surface morphology of pure CdO, CdO/La_2O_3 and CdO/La_2O_3/PVP nanocomposites. Pure CdO nanoparticles exhibits homogenously cubical crystal structure and all particles are attached closely with each other which show in figure 3a. Figure 3b-c shows the variations in morphology due to the incorporation of La_2O_3 and PVP in CdO. In figure 3c, the SEM images shows the irregular thin plates with less agglomeration for PVP added CdO/ La_2O_3. This reduced agglomeration attributes to surfactant PVP which used to stabilize the atoms in surface. It is noticed that size of the CdO/La_2O_3 and CdO/La_2O_3/PVP binary nanocomposites decreases due to nucleation effect which same as in our XRD result. The significant reduction of particle size and less agglomeration in CdO/La_2O_3 and CdO/La_2O_3/PVP nanocomposites may be attributes to interaction of lanthanum oxide and PVP with CdO lattice. Hence it is confirmed that the addition of lanthanum oxide and PVP influences the size and morphology of CdO nanoparticles which is also confirmed with XRD results.

The elements present and its composition percentage in the synthesized samples are confirmed by using energy dispersive spectroscopy (EDS). The EDS spectra in figure 4a, confirms the presence of Cd and oxygen in pure CdO. Further, the figure 4 (b-c) shows the existence of Cd, O, and in La in CdO/$La_2O_3$and CdO/La_2O_3/PVP samples. Furthermore, EDS spectra authenticate the synthesize of binary heterogenous CdO/La_2O_3 and CdO/La_2O_3/PVP nanocomposites. Table 1 represents the atomic weight percentage of elements present in the all three synthesized samples. This EDS result is in well synchronized with our XRD and SEM analysis.

Table 1 Atomic concentration of elements for pure CdO, CdO/ La_2O_3 and CdO/La_2O_3/ PVP nanocomposites measured from the EDS analysis

Compound Name	Atomic % of Cd	Atomic % of La	Atomic % of O
CdO	62.15	--	37.85
CdO/ La_2O_3	42.58	30.16	27.26
CdO/ La_2O_3/ PVP	41.20	32.64	26.16

To further confirm the heterogeneous structure at atomic scale, TEM images are taken for pure CdO, CdO/La_2O_3 and CdO/La_2O_3/PVP nanocomposites which are shown in figure 5 (a-f). The TEM images confirm the polycryatalline cubical crystal structure of synthesized samples. Figure 5 (c-f) images confirm that lanthanum oxide and PVP were exists on the surface of CdO lattice. Additionally, the selected area electron diffraction (SAED) pattern shows bright patches which

reveals that the nanocomposite is high crystalline nature with cubic structures. The SAED pattern also confirms that the existing diffraction peaks are corresponds to CdO and La_2O_3. Furthermore, the SAED confirms that the lattice inter planar d spacing related the CdO and La_2O_3 nanoparticles. TEM images confirm that the surfactant PVP reduces the agglomeration effect and reduces the particle size which is concurrence with our XRD and SEM reports.

3.4 UV-Vis Absorption Studies

The optical transmittance and bandgap analysis of the nanomaterials is imperative factor for its optoelectronic and photovoltaic applications. The impact of lanthanum oxide and PVP in optical behavior of the CdO nanocomposites at room temperature is studied by UV absorption spectra. Figure 6 shows the absorption transmittance spectra of CdO, CdO/La_2O_3 and CdO/La_2O_3/PVP nanocomposites at room temperature. All the three synthesized samples are transparent to visible region [4]. The absorbance value in the visible region increases for pure CdO and decreases for CdO/La_2O_3 and CdO/La_2O_3/PVP nanocomposites. The broad absorbance in visible region for CdO/La_2O_3 and CdO/La_2O_3/PVP nanocomposites suggest that this is a promising material for visible light absorption process [36].

To acquire better approaching in electronic structure, the optical band gap energy of the nanoparticles was determined by Tauc's equation. The process of electronic transitions and the band structure in the nanocomposite depends on optical absorption coefficient and photon energy.

$$\alpha h\nu = A\,(h\nu - Eg)^{\frac{1}{2}}$$

Where α = Optical absorption coefficient, A is constant (0.9) and photon energy is hν.

In figure 7, the graph is plotted with $(\alpha h\nu)^2$ versus photon energy and the optical band gap value (E_g) is calculated. The obtained band gap value of pure CdO is 3.4 eV. This band gap value is red shifted to 3.95 eV and 4.2 eV for CdO/La_2O_3 and CdO/La_2O_3/PVP nanocomposites respectively. The increase in band gap due to incorporation of La_2O_3 and PVP with decrease in particle size which is already confirmed in our XRD results. Further, this enlargement in band gap value is explained by Burstein-Moss (B-M) effect. According to B-M effect, the increase in carrier concentration due to the addition of La_2O_3 and PVP into CdO lattice gives the increase in band gap value [2]. But in pure CdO sample, no free charge carriers due to the ionic bond between Cd^{2+} and O^{2-}. In general, the parameters such as particle size, synthesis conditions, structural defects, oxygen vacancies and high carrier concentration gives impact on variations in band gap value [21, 26,14]. Finally this absorption studies concluded that synthesized CdO/La_2O_3 and CdO/ La_2O_3/PVP nanocomposites with tunable band gap is the suitable materials for optoelectronic and solar cell applications.

3.5 Photoluminescence Study

Photoluminescence study is an authoritative characterization method to determine the electronic structure, recombination of electron-hole Pair and energy band level of nanocomposites. Figure 8 a&b shows the photoluminescence spectra of pure CdO, CdO/La_2O_3 and CdO/La_2O_3/PVP nanocomposites at room temperature. The paeks at 341 nm for pure CdO, 361 nm for CdO/La_2O_3 and CdO/La_2O_3/PVP nanocomposites correspond to near band edge emission (NBE) which is attributes to excitonic recombination [21]. Also the increase in intensity of NBE for La_2O_3 and PVP added nanocomposites confirms that the incorporation of dopants into CdO. The violet emission in the region between 432 nm to 460 nm for the all three synthesized samples arises due to recombination of electron-hole pair centers from intrinsic or extrinsic defects [1, 8, 40]. In PL spectra of CdO/La_2O_3 and CdO/La_2O_3/PVP nanocomposites, the intensity of violet emission is increases compared to pure CdO which attributes to the defect levels of lanthanum 4f orbital to O-2p bands. The green emission peak at 529 nm for all three synthesized samples is correspond to electron-hole pair in oxygen and metal vacancies [2, 38]. The second green emission peaks are observed at 599 nm for pure CdO and 573 nm for CdO/La_2O_3 and CdO/La_2O_3/PVP nanocomposites. This second peak might be corresponds to oxygen vacancies and transition between valence band and conduction band [8, 38]. The red emission peak with increased intensity in CdO/La_2O_3 and CdO/ La_2O_3/PVP nanocomposites is due to deep trap emission. These results are harmonized with our XRD and UV results. This PL studies, confirms that the CdO/La_2O_3 and CdO/La_2O_3/PVP nanocomposites with enhanced photo luminescence properties are the suitable materials in photo catalytic applications and nanoelectronics.

3.6 CIE Chromaticity Diagram

Emerging the novel luminescent materials is a fast desire to overcome the demands in various applications such as indoor lighting, display devices and wearable electronics. The Nanocomposites matrix of semiconductor oxides, rare-earth metal oxides and Polyvinylpyrrolidone (PVP) would be the promising next-generation solid-state lighting source which can entirely exhausted the traditional incandescent lamps, fluorescence lamps and conventional lighting devices due to their merits of low electricity consumption, long lifetime and compact in size [42]. Color coordinate diagram of the synthesized nanocomposite phosphors are analyzed using computed imaging software available in the CIE 1931 color chromaticity diagram. Figure 8(c) shows the CIE 1931 color coordinated diagram of CdO, CdO/La_2O_3 and CdO/La_2O_3/PVP nanocomposites. The calculated color coordinates (x, y) are found to be (0.33, 0.33), (0.37, 0.35) and (0.31, 0.38) for CdO, CdO/La_2O_3 and CdO/La_2O_3/PVP nanocomposites, correspondingly. Clearly, the color coordinates of CdO and CdO/La_2O_3 nanocomposites have been placed in the strong white region of the CIE diagram, while the CdO/La_2O_3/PVP nanocomposites has been slightly tuned to the green region. The color coordinates of these phosphors are strongly agreed with standard value of white region (0.310, 0.316) of the National Television Standard Committee (NTSC) [43]. These results have revealed that the prepared nanocomposites exhibits excellent CIE chromaticity properties and hence they would have potential application in white light emitting phosphors.

3.6 Magnetic Studies

The magnetic measurement of synthesized sample gives specifics the interactions between synthesized metal ions and type of magnetic materials from which we can find the promising

materials for various technological applications. Figure 9 shows the magnetization versus applied field (M-H) curves of the synthesized samples pure CdO, CdO/La_2O_3 and CdO/La_2O_3/PVP nanocomposites at room temperature. From this figure 9, we can conclude that the magnetic properties such as retentivity, coercivity and saturated magnetization depend on incorporated nanoparticles La_2O_3 and PVP. Pure CdO nanoparticles show the good ferromagnetic properties. On other side, M-H curve of CdO/La_2O_3 binary nanocomposites reveals super paramagnetic nature. But interestingly CdO/La_2O_3/PVP nanocomposites show the weak ferromagnetic property [44]. The coercivity value for pure CdO is 460.85 Oe and it get reduces for CdO/La_2O_3 and CdO/ La_2O_3/PVP nanocomposites. The retentivity value of pure CdO is high when compared to CdO/ La_2O_3 and CdO/La_2O_3/PVP nanocomposites.

Further, the processes like magnetic interactions and Vander walls force involving in the particles and also the production of dangling bonds are leads to particle agglomeration. Agglomeration is reduced in our synthesized CdO/La_2O_3/PVP nanocomposites due to capping agent PVP which also in harmony with our SEM results. This confirms that the week ferromagnetic CdO/La_2O_3 and CdO/La_2O_3/PVP nanocomposites could arises from oxygen vacancy and surface morphology changes due the incorporation of La_2O_3 and PVP [45,46]. It is observed that magnetization value is decreased for pure CdO when compared to CdO/La_2O_3 and CdO/ La_2O_3/PVP nanocomposites. This confirms that the incorporation of La_2O_3 and PVP on CdO lattices. The drop in particle size in CdO/La_2O_3 and CdO/La_2O_3/PVP nanocomposites promotes the interactions between La 4f electron with Cd ions which gives week ferromagnetic nature [45,47]. In other words, the impurity present on surface of synthesized CdO/La_2O_3 and CdO/ La_2O_3/PVP nanocomposites might be gives week ferromagnetic nature which also confirmed in our XRD results. Since sample with large magnetization value is the promising materials for spintronics, CdO/La_2O_3 and CdO/La_2O_3/PVP nanocomposites are promising material in spintronics.

Table 2 Magnetic measurements data for pure CdO, CdO/La_2O_3 and CdO/La_2O_3/PVP nanocomposites from the VSM analysis

Compound Name	Coercivity H_c (Oe)	Remanent Magnetization M_r 10^{-6} in emu/g	Saturation Magnetization(M_{Hmax}) in 10^{-3}emu/g
CdO	460.85	459.5	1.888
CdO/ La_2O_3	341.62	47.728	1.92
CdO/La_2O_3/ PVP	187.50	108.72	2.4390

3.7 Dielectric Studies

Dielectric measurements are a powerful performance for analyzing the relaxation and conduction properties in synthesized samples. In order to analyze the dielectric behavior of the samples, the synthesized materials were formed as pellets using pelletizer. The silver paste was applied on both surfaces of the sample, which acts as an electrode. The dielectric measurements were carried out using the two-probe setup. The chamber used for the analysis was evacuated and filled with helium gas before the commencement of the measures to avoid adsorption of moisture on the surface of

the sample. The dielectric constant of the synthesized samples is dependent on dielectric polarization due to applied electric field.

Figure 10 (a-c) shows the frequency needy variant in dielectric constant for pure CdO, CdO/La_2O_3 and CdO/La_2O_3/PVP nanocomposite at room temperature. As the frequency of the applied electric field increases, dielectric constant decreases for CdO, CdO/La_2O_3 and CdO/La_2O_3/PVP nanocomposite. This reduction in dielectric constant is speedy at low frequency and steady at high frequency. In general at high frequencies, the internal dipoles are not able to align themselves effortlessly which attributes to the reduction in dielectric constant [7, 31, 48]. The decrease in dielectric constant at high frequency for CdO/La_2O_3 and CdO/La_2O_3/PVP nanocomposite is arises from less interconnected system formation (accumulation of charge carriers at boundaries) due to heterogeneity of the synthesized nanocomposite. The process behind the increase in dielectric constant at lower frequency is space charge polarization which is responsible for electrostatic binding strength [22]. However, the dielectric constant value is very much greater for pure CdO nanoparticles when compared with CdO/La_2O_3 and CdO/La_2O_3/PVP nanocomposite.

Figure 11(a-c) represents the electrical conductivity variation with frequency of the synthesized pure CdO, CdO/La_2O_3 and CdO/La_2O_3/PVP nanocomposite at room temperature. The electrical conductivity value is much more for CdO/La_2O_3 and CdO/La_2O_3/PVP nanocomposite than pure CdO samples. The incorporation of La_2O_3 and PVP on CdO lattice increases the free charge carriers and hence electrical conductivity is increases for $CdO/La_2O_3$and CdO/La_2O_3/PVP nanocomposite [24]. On others side, the electrical conductivity value is found to increase with an increase in the frequency CdO/La_2O_3 and CdO/La_2O_3/ PVP nanocomposite. The observed increase of electrical conductivity with an increase in the frequency is attributed to the dominance of the ionic conduction in the CdO/La_2O_3 and CdO/La_2O_3/PVP nanocomposite.

The parameter dielectric loss is the measurement of the ratio of dissipated energy to the total energy stored by a dielectric material when external electric field is applied. The dielectric loss of materials is takes place by the various processes such as conduction, space charge polarization and other dissipative phenomenon. Figure 12(a-c) reveals the variation of dielectric loss with frequency for pure CdO, CdO/La_2O_3 and CdO/La_2O_3/PVP nanocomposite at room temperature. The dielectric loss value is high at low frequency and decreases exponentially then stable at high frequency. In practical applications of electronic devices, we need materials with high dielectric constant and low dielectric loss. In this research work, CdO/La_2O_3/PVP nanocomposite having high dielectric constant and low dielectric loss and therefore can be used as emergent materials in electronic devices.

.

3.8 EMI Shielding

In general, the nanocomposite with both magnetic and electrical properties is used as EMI shielding material. The basic mechanisms involved in EMI shielding are reflection and absorption of electromagnetic radiation by the samples which blockade the passing of electromagnetic radiation. If the shielding material possesses the more charge density which can interact with electromagnetic radiation and it reflects the radiation. On other side the absorption of electromagnetic radiation is takes place in magnetic materials. The condition to get efficient EMI shielding is material should have minimum refection and maximum absorption of electromagnetic

waves which comes from the properties of high conductivity, magnetic permeability and synthesized sample thickness [22, 25]. When the electromagnetic waves incident on the synthesized samples, some of incident energy is reflected and absorbed and some gets transmitted through samples. EMI SE is calculated from the ratio of incident power to transmitted power and is defined below

$$\text{SE (dB)} = 10 \log \frac{\text{P incident}}{\text{P transmitted}} - - - - - - - - - - - (1)$$

Hence the total shielding effectiveness (SE) is given by the relation

$$SE_{TOT} = SE_{Ref} + SE_{Abs} - - - - - - - - - - - - - - - (2)$$

Where SE_{TOT} represents total shielding efficiency due to both absorption and reflection, SE_{Ref} refers shielding due to reflection and SE_{Abs} is shielding due to absorption.

The value of reflection of radiation in SE is calculated by

$$\text{SE}_{\text{ref}} = 20\ log \left[\frac{\left(\frac{\sigma_{ac}}{\omega_H \varepsilon_o \mu_r} \right)^{\frac{1}{2}}}{4} \right] - - - - - - - - - - - - - (3)$$

and the value of absorption of radiation in SE is given by

$$\text{SE}_{\text{abs}} = 20\ log \left[exp\left(\frac{t}{\delta} \right) \right] \text{(dB)} - - - - - - - - - - - - - - - (4)$$

The refection process is only depends on conductivity and magnetic permeability, but the absorption process is depends on conductivity, magnetic permeability and synthesized sample thickness.

Where, $\omega_H = 2\pi f_H$ is angular frequency, ε_o is the permittivity of free space, $\mu_r$is the relative permeability, t represents sample thickness, δ is the skin depth and it is given by

$$\delta = \left[\frac{2}{\omega_H \mu \sigma_{ac}} \right]^{\frac{1}{2}} - - - - - - - - - - - - - - - - - - (5)$$

The SE variation with frequency for pure CdO, CdO/$La_2O_3$and CdO/La_2O_3/PVP nanocomposite is shown in figure 12 (a-c). From the figure it was observed that the SE value of CdO, CdO/ $La_2O_3$and CdO/La_2O_3/PVP nanocomposite is 51, 72 and 78 dB respectively at the 6.6 frequency. In all three samples, at low frequency, electromagnetic shielding effectiveness is increases and at high frequency it gets decreases. In practical, at high frequency the electromagnetic wave has more penetrating power than at low frequency. Hence there is a reduction in electromagnetic shielding

effectiveness at high frequency [49]. Further, at low frequency, the increase in electromagnetic shielding effectiveness is attributes to reflection loss. Xuan et al results observed that the addition of rare earth element lanthanum in Ni-P alloy increases the SE due to its microcosmic electron structure [50].

The parameters such as particle size and morphology of the samples also will affect the SE. Vineetha Shukla review works confirms that the nanocomposites with greater particle size will improves the shielding efficiency [51]. CdO/La_2O_3 and CdO/La_2O_3/ PVP nanocomposite show comparatively high SE than pure CdO samples. This may be attributes from large particle size of CdO/La_2O_3 and CdO/La_2O_3/PVP than pure CdO. Among three synthesized samples, CdO/La_2O_3/ PVP nanocomposite show high SE is due to its high conductivity (more charge carriers) of the PVP which is already exists with our dielectric results [51].

3.9 Photocatalytic Activities

In present technical life style, the development in textile industry produces the dye contamination (Methylene blue, Methyl Orange) which leads to major environmental pollution. Hence the recent research trends try to find the efficient method to remove environmental pollutant. Figure 14 (a-c) depicts the photocatalytic activity of pure CdO, CdO/La_2O_3 and CdO/La_2O_3/PVP nanocomposite for the degradation of MB dye at various time periods under UV light irradiation. For all three synthesized samples the absorption peak intensity decreases with increase of irradiation time. Figure 15(a) reveals the efficiency of the pure CdO, CdO/La_2O_3 and CdO/La_2O_3/PVP nanocomposite on effect of absorbance change in MB dye at various time intervals. In the dark experiment, no effect of absorbance change in MB dye was observed.

Figure 15 (b) shows the degradation percentage of dye for pure CdO, CdO/La_2O_3 and CdO/La_2O_3/PVP nanocomposite. By using equation1, the values of photocatalytic degradation feeiciency are calculated. After 120 min of irradiation time, methylene blue dye degradation efficiency is achieved 22.85%, 48% and 65.77% respectively for pure CdO, CdO/La_2O_3 and CdO/La_2O_3/PVP nanocomposite. The high photocatalytiv degradation efficiency is achieved in CdO/La_2O_3 and CdO/La_2O_3/PVP compared to pure CdO. This attributes to the more number of surface activators present in La_2O_3 and PVP added samples due to its reduction in particle size [52]. Further, from many research results we observed that the addition of rare-earth metals reduce the electron-hole recombination process and thereby increase the photocatalytic efficiency [53, 54]. The photo degradation reaction kinetics of MB dye in all synthesized nanocomposite is shown in figure 15 (c). The pseudo-first-order kinetic reaction $-\log (C_t/C_0)$ of the all synthesized samples is linear with the irritation time. Hence we concluded that the particle size, surface to volume ratio, bandgap value and proper selection of dopants are tuning the efficiency of photocatalytic activity.

3.9.1 Photocatalytic Mechanism

The schematic representation of photocatalytic mechanism of CdO, CdO/La_2O_3 and CdO/La_2O_3/PVP nanocomposite is shown in figure 16. The increased efficiency of photocatalytic activity in CdO/La_2O_3 and CdO/La_2O_3/PVP nanocomposites corresponds to three factors such as UV light absorbance; reduce the electron-hole recombination and particle size. To analyze the reduction in electron-hole recombination process, the conduction band (CB) and valence band

(VB) edge location of the CdO and La_2O_3 semiconductors are evaluated from the following equations:

$$E_{CB} = \chi - \text{Ee} - 0.5\text{Eg} \quad \text{----------6}$$

$$E_{VB} = E_{CB} + \text{Eg} \quad \text{----------7}$$

The electro negativity (χ) of CdO is 5.71eV and for La_2O_3 is 5.28eV [55].

E_e is the free electrons energy on the hydrogen scale (4.5eV). E_g is the band gap of the CdO

and La_2O_3 nanoparticles. By using above equations, the band edge values CdO and $La2O_3$ semiconductors are calculated and shown in the Table 3.

Table 3. Calculation of Band edge position

Catalyst	Electro negativity (χ) (eV)	E_{CB} (eV)	E_{VB} (eV)	E_g (eV)
CdO	5.71	-0.590	3.01	3.6
La_2O_3	5.28	-1.37	2.93	4.3

During UV light irradiation, the electrons in the valence band of CdO and La_2O_3 nanocomposites progress to the conduction band, which creates an equal number of holes in the valence band. The free electrons in the conduction band of CdO and La_2O_3 act in response with oxidation to produce superoxide anion (O^{2-}) radicals. Further, the hole in the valence band reacts with free water molecule which generates hydroxyl radicals (OH^-). These superoxide anion and hydroxyl radicals react with MB dye molecules and make it to degrade by releasing CO_2 and H_2O.

$CdO + h\nu \rightarrow CdO\ (e^-_{CB} + h^+_{VB})$

$CdO\ (e^-_{CB}) + La_2O_3 \rightarrow CdO + La_2O_3\ (e^-_{CB})$

$La_2O_3\ (e^-_{CB}) + O_2 \rightarrow La_2O_3 + O^{2-}$

$La_2O_3\ (h^+_{VB}) + CdO \rightarrow. \ La_2O_3 + CdO\ (h^+_{VB})$

$CdO\ (h^+_{VB}) + H_2O \rightarrow. \ OH^- + H^+$

$O_2^- / OH^- + \text{dye (MB)} \rightarrow \text{oxidative decomposition} \rightarrow CO_2 + H_2O$

Finally, this result concluded that, the photocatalytic efficiency of CdO/ La_2O_3/PVP nanocomposites is high and which turn it as promising materials in various industry to remove organic pollutants.

4. Conclusion

This research work paves the pathway to come together the advantages of the lanthanum oxide and CdO with PVP polymeric binder to enrich the opical, dielectric, magnetic and EMI shielding properties. The XRD analysis confirms the heterogeneous formation of both CdO and La_2O_3 nanocomposites. The addition of La_2O_3 and PVP would tune the bandgap value which attributes to absorption of various wavelength of solar energy for solar cell applications. The photoluminescence studies identified that the synthesized nanocomposites shows the properties of white light emitting phosphors. The week ferromagnetic nature of CdO/La_2O_3 and CdO/ La_2O_3/PVP nanocomposites could arises from oxygen vacancy and surface morphology changes due the incorporation of La_2O_3 and PVP. The dielectric studies indicating that the La_2O_3 and PVP incorporated sample having high dielectric constant, electrical conductivity and low dielectric loss due to its increase in free charge carriers. CdO/ La_2O_3/PVP nanocomposite show high EMI SE is due to its high conductivity. The incorporation of lanthanum oxide and PVP reduces the electron-hole recombination process and hence enhance the photocatalytic degradation efficiency of MB dye under UV light. Therefore, from the observed results, it has been concluded that the binary nanocomposite of CdO and lanthanum oxide with the polymer matrix PVP provide a new way to enhances the optical, electrical, photocatalytic and EMI SE in various electronic applications.

References

1. Aswani, V. Pushpa Manjari, B. Babu, Sk. Muntaz Begum, G. Rama Sundari, K. Ravindranadh, R.V.S.S.N. Ravikumar, J Molecular St, 2014, 1063, 178–183
2. P. Sakthivel · S. Asaithambi · M. Karuppaiah · S. Sheikfareed · R. Yuvakkumar · G. Ravi J Materials Science: Materials in Electronics 2019, 30, 9999-10012.
3. Abdollah Eskandari, Farid Jamali-Sheini, Mohsen Cheraghizade Ramin Yousefi Applied Nanoscience, 2018, 8 (5), 937-948
4. Domenico A. Cristaldi, Salvatrice Millesi, Isodiana Crupi,Giuliana Impellizzeri,Francesco Priolo, Robert M. J. Jacobs, Russell G. Egdell, and Antonino Gulino J. Phys. Chem. C 2014, 118, 15019 − 15026.
5. H.-Y. He and J. Lu, MRS Communications 2013, 3, 47–50
6. R.K. Gupta, K. Ghosh, R. Patel, P.K. Kaho, J Alloys Comp, 2011, 509, 4146–4149
7. Pratima Makwana Davit Dhruv Sapana Solanki Hetal Boricha1 A. Satyaprasad M. Ranjan P. S. Solank N. A. Shah, Journal of Sol-Gel Science and Technology, 2019,89,866-875.

8. Md Abdus Subhan,, Abul Monsur M. Fahima, Pallab Chandra Saha, Mohammed M. Rahmanb, Kulsuma Begumc, Abul Kalam Azad , Nano-Structures & Nano-Objects, 2017, 10, 30–41
9. S. Sudheer Khan Journal of Photochemistry and Photobiology B: Biology, 2014, 142, 1-7
10. Ganesan Anandha babu, Ganesan Ravi, Thaiyan Mahalingam,Mani Navaneethan, Mukkannan Arivanandhan,§ and Yasuhiro Hayakawa, J. Phys. Chem. C 2014, 118, 23335−23348.
11. N. Sahu and R. K. Duchaniya Journal of Materials Science & Surface Engineering, 2013, 1(1), 11-14.
12. S. de Castro , S.L. dos Reis, A.D. Rodrigues, M.P.F. de Godoy, Materials Science and Engineering B, 2016, 212, 96–100
13. A.B. Bodade, A.M. Bende, G.N. Chaudhari, Vacuum, 2008, 82, 588–593
14. Kunjie Wang, YanpingWua, Hongxia Li , Mingliang Li, Feng Guana, Haiyan Fan Journal of Inorganic Biochemistry, 2014, 141, 36–42.
15. R. Saravanan, F. Gracia , Mohammad Mansoo Khan , V. Poornima , Vinod Kumar Gupta, V. Narayanan g, A. Stephen, Journal of Molecular Liquids, 2015, 209, 374–380
16. H. Sivaram, D. Selvakumar, A. Alsalme, A. Alswieleh, R. Jayavel, Journal of Alloys and Compounds, 2017, 731, 55-63
17. M. Uma, N. Balaram, P.R. Sekhar Reddy, V. Janardhanam, V. Rajagopal Reddy, Hyung-Joong Yun, Sung-Nam Lee, And Chel-Jong Choi, Journal of Electronic Materials, 2019, 48(7), 4217-4225
18. Jean-Claude G. Bunzli , Steve Comby, Anne-Sophie Chauvin, Caroline D. B. Vandevyver, Journal Of Rare Earths, 2007, 25, 257 – 274
19. Qiuping Li, Bing Yan, J Rare Earths 2019, 37, 113-123.
20. Maryam Ranjbar, Mostafa Yousefi, , J Inorg Organomet Polym, 2014, 24, 652–655
21. C. Maria Magdalane, K. Kaviyarasu, N. Matinise, N. et al South African Journal of Chemical Engineering, 2018, 26, 49-60
22. Aqib Muzaffar , M. Basheer Ahamed , Kalim Deshmukh & S. K. Khadheer, Pasha, Polymer-Plastics Technology and Materials, 2020, 59, 1667-1678.
23. Bo Wen , Maosheng Cao , Mingming Lu , Wenqiang Cao , Honglong Shi , Jia Liu, et al, Adv. Mater. 2014, 26, 3484–3489.
24. Kambiz Chizari, Mohammad Arjmand, Zhe Liu, Uttandaraman Sundararaj, Daniel Therriault, Materials Today Communications, 2017, 11,112-118.
25. M. Gurusiddesh, B. J. Madhu, G. J. Shankaramurthy , Journal of Materials Science: Materials in Electronics, 2018,29,3502-3509
26. Kalim Deshmukh, M. Basheer Ahamed, Kishor Kumar Sadasivuni, Deepalekshmi Ponnamma, Rajendra R. Deshmuk, J. Polym Res, 2017 24, 1-14
27. Paulose Thomas and K. E. Abraham, J. Adv. Dielectrics, 2016, 6, 1650030(1-8).
28. Tamita Rakshit, Indranil Manna, and Samit K. Ray,J. App Phy, 2015, 117, 025704.
29. M. Ali Yıldırım, Sumeyra Tuna Yıldırım, Emine Fedakar Sakar, Aytunc Ates Spectrochimica Acta Part A: Molecular and Biomolecular Spectroscopy, 2014, 133, 60–65.
30. HongWei Zhaoa, YuanLiang Lib, ChunRui Changa, ChunLiang Yan, Mat. Res, 2016, 19,

31. Masoud Ebrahimzadeh, Mehrnoush Nakhaei, Mansoure Padam, Ali Bahari, Proc. Natl. Acad. Sci., India, Sect. A Phys. Sci. 2020, 90,637-646,
32. A.M. El Sayed, S. El-Sayed,W.M. Morsi, S. Mahrous, A. Hassen, Polymer Composites, 2014.35, 1842-1851.
33. Idalia Bilecka and Markus Niederberger, Microwave chemistry for inorganic nanomaterials synthesis, Nanoscale, 2010, 2, 1269-1528,
34. Neha Jain, Rajan Kumar Singh · Khalid Bin Masood, Jai Singh, Applied Sciences, 2020,2, 410
35. Daniela Salinas, Catherine Sepúlveda, Néstor Escalona, J. L. GFierro, Gina Pecchi Journal of Energy Chemistry, 2018, 27,565-572
36. Karunamoorthy Saravanakumar, Subramani Muthupoongodi , Velluchamy Muthuraj, Journal of Rare Earths, 2019, 37, 853-860
37. Ahmad Umar, M.S. Akhtar, M.S. Al-Assiri, A.E. Al-Salami, S.H. Kim, Ceramics International, 2017, 43, 11753-11758
38. Naif Mohammed Al-Hada, EliasSaion, Halimah Mohamed Kamari, Moayad Husein Flaifel,et al, Materials Science in Semiconductor Processing, 2016, 53, 56–65
39. Abderrafik Nemamcha Jean-Luc Rehspringer, and Djameledine Khatmi, J. Phys. Chem. B, 2006, 110, 383-387.
40. Naif Mohammed Al-Hada, Elias Saion, Zainal Abidin Talib and Abdul Halim Shaari, Polymers 2016, 8, 113
41. H. Yang, X. Peng, C. Cao, L. Wu, N. Chen, X. Zhang, W. Xie, Q. Tong and Z. Wu, Organic Electronics, 2020, 85, 105848
42. L. Chen, C.C. Lin, C.W. Yeh and R.S. Liu, Materials 2010, 3(3), 2172-2195.
43. S. Senthil, S. Srinivasan, T. Thangeeswari, M. Silambarasan and V. Ratchagar, Journal of Superconductivity and Novel Magnetism, 2020, 33, 2469–2481.
44. Mohammad Ahmed-Fouad Basha, Polymer Journal, 2010, 42, 728-734,
45. Ganesan Anandha babu, Ganesan Ravi, Thaiyan Mahalingam, Mani Navaneethan, Mukkannan Arivanandhan, and Yasuhiro Hayakawa J. Phys. Chem. C 2014, 118, 23335−23348.
46. K. Srinivas,M. Vithal, B. Sreedhar M. Manivel Raja, and P. Venugopal Reddy, J. Phys. Chem.C 2009, 113, 3543–3552
47. G. Anandha babu, Y. Hayakawa, G. Ravi, Materials Letters, 2015, 149, 54-57
48. Shyamapada Shit, Animesh Layek , J Mater Sci:Mater Electronics, 2016,27,3435-3442.
49. Monika Saini· Rajni Shukla S. K. Singh, Journal of Inorganic and Organometallic Polymers and Materials 2019,4,1639-1648.
50. Xuan Tianpeng, Yang Guangzhou, Yang Lilin, Ju Zhengting, Journal of Rare Earths, 24, 2006, 389-392.
51. Vineeta Shukla, Nanoscale Adv., 2019, 1, 1640-1671.
52. Elayaraja M, Karthrainal Punithavathy, M Jothibas, Muthuvel A, Johnson Jeyakumar, Nanotechnology for Environmental Engineering, 5, 1-10, 2020
53. Himanshu Narayan, Hailmichael Alemu, Lijeloang Setofolo, and Lebohan, International Scholarly Research Network Physical Chemistry, 2011,2012, 1-9.
54. Y. Ikuma and V.Muruesan, , International Journal of Photoenergy, 2011,2012, 1-10.
55. Yong Xu And Martin A.A. Schoonen, American Mineralogist, 85, 543–556, (2000)

Figure Captions:

Figure 1 - XRD patterns of pure CdO, CdO/La_2O_3 and CdO/La_2O_3/ PVP nanocomposites

Figure 2 - FTIR spectra of pure CdO, CdO/La_2O_3 and CdO/La_2O_3/PVP nanocomposites.

Figure 3 - Scanning electron micrographs of (a) pure CdO, (b) CdO/La_2O_3 and (c) CdO/La_2O_3/PVP nanocomposites

Figure 4(a-c) - Energy dispersive spectra of (a) pure CdO, (b) CdO/La_2O_3 and (c) CdO/La_2O_3/ PVP nanocomposites.

Figure 5(a-f) - TEM and SAED images of pure CdO (a&b), CdO/La_2O_3 (c & d) and CdO/La_2O_3/ PVP (e&f) nanocomposites

Figure 6 - UV-Vis absorption spectra of pure CdO, CdO/La_2O_3 and CdO/La_2O_3/ PVP nanocomposites

Figure7 - Band gap spectra of pure CdO, CdO/La_2O_3 and CdO/La_2O_3/ PVP nanocomposites .

Figure 8(a) - PL spectra of pure CdO nanoparticles

Figure 8(b) - PL spectra of CdO/La_2O_3 and CdO/La_2O_3/ PVP nanocomposites

Figure 8 (c) - CIE chromaticity diagram of CdO, CdO/La_2O_3 and CdO/La_2O_3/PVP nanocomposites

Figure 9 - Magnetization hysteresis (M-H) curves of pure CdO, CdO/La_2O_3 and CdO/La_2O_3/PVP nanocomposites

Figure 10 (a-c) - Dielectric constant for pure CdO, CdO/La_2O_3 and CdO/La_2O_3/PVP nanocomposite at room temperature

Figure 11 (a-c) - Electrical conductivity with frequency of CdO, CdO/La_2O_3 and CdO/La_2O_3/ PVP nanocomposite at room temperature.

Figure 12 (a-c) - Dielectric loss of CdO, CdO/La_2O_3 and CdO/La_2O_3/PVP nanocomposite

Figure 13 - EMI shielding Effectiveness of CdO, CdO/La_2O_3 and CdO/La_2O_3/PVP nanocomposite

Figure 14 (a-c) - Time dependent absorbance spectra (a) pure CdO, (b) CdO/La_2O_3 and (c) CdO/La_2O_3/PVP nanocomposite

Figure 15 (a) - Photocatalytic degradation analysis curves of pure CdO , CdO/La_2O_3 and CdO/La_2O_3/ PVPnanocomposites

Figure 15 (b) - Photocatalytic degradation efficiency analysis curves of pure CdO CdO/La_2O_3 and CdO/La_2O_3/PVP Nanocomposites

Figure15 (c) - Kinetic curve study of photocatalytic degrdation of MB dye in pure CdO. CdO/La_2O_3 and CdO/ La_2O_3/PVP nanocomposites

Figure 16 - The schematic representation of photocatalytic mechanism of CdO, CdO/La_2O_3 and CdO/La_2O_3/PVP nanocomposite

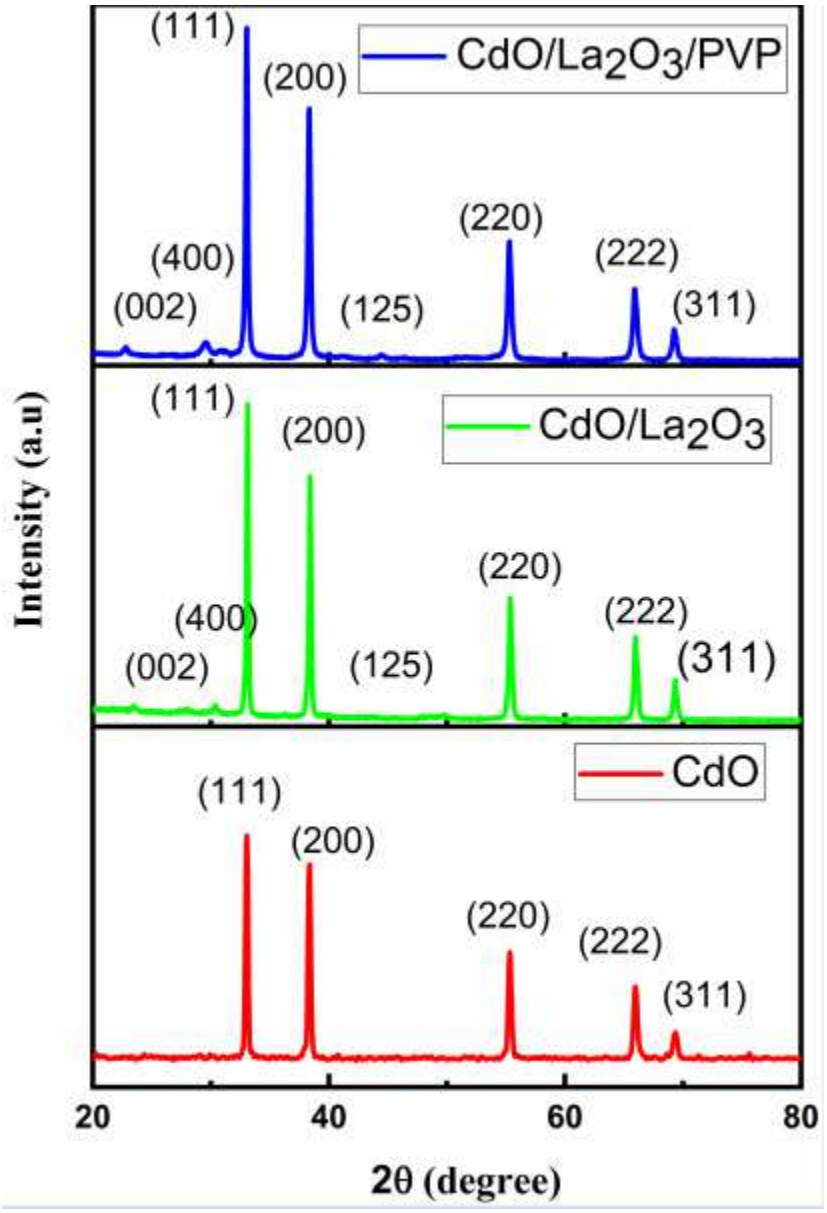

Figure 1 **XRD patterns of pure CdO, CdO/La_2O_3 and CdO/ La_2O_3/ PVP nanocomposites**

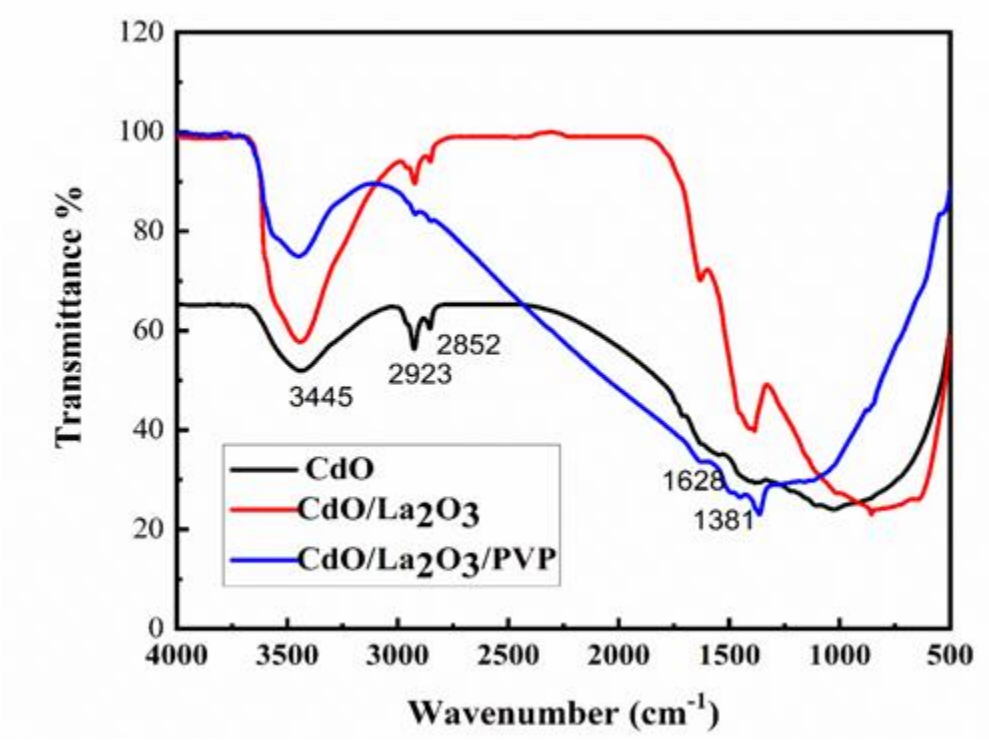

Figure 2 FTIR spectra of pure CdO, CdO/La_2O_3 and CdO/La_2O_3/PVP nanocomposites

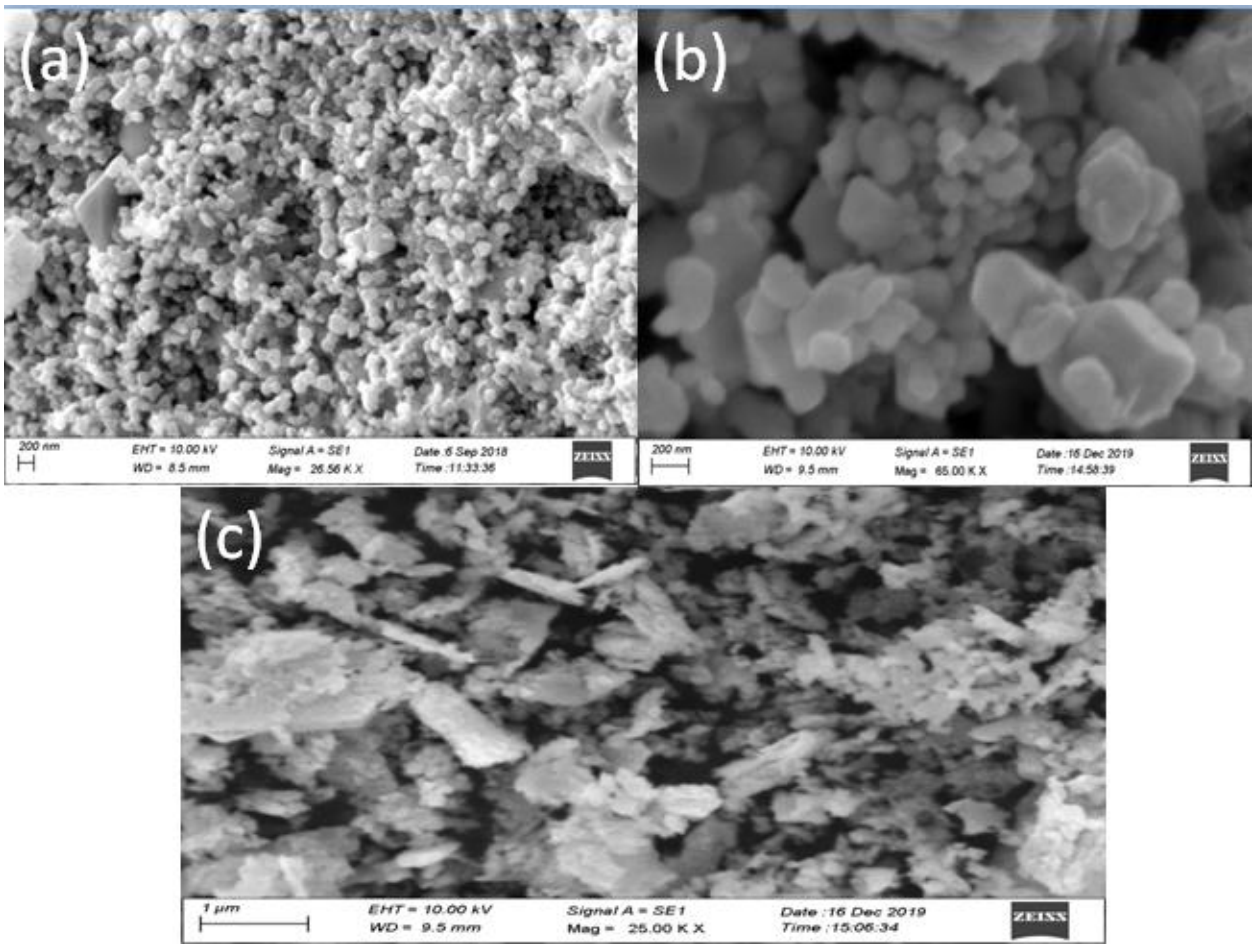

Figure 3 **Scanning electron micrographs of (a) pure CdO, (b) CdO/ La_2O_3 and (c) CdO/ La_2O_3/PVP nanocomposites**

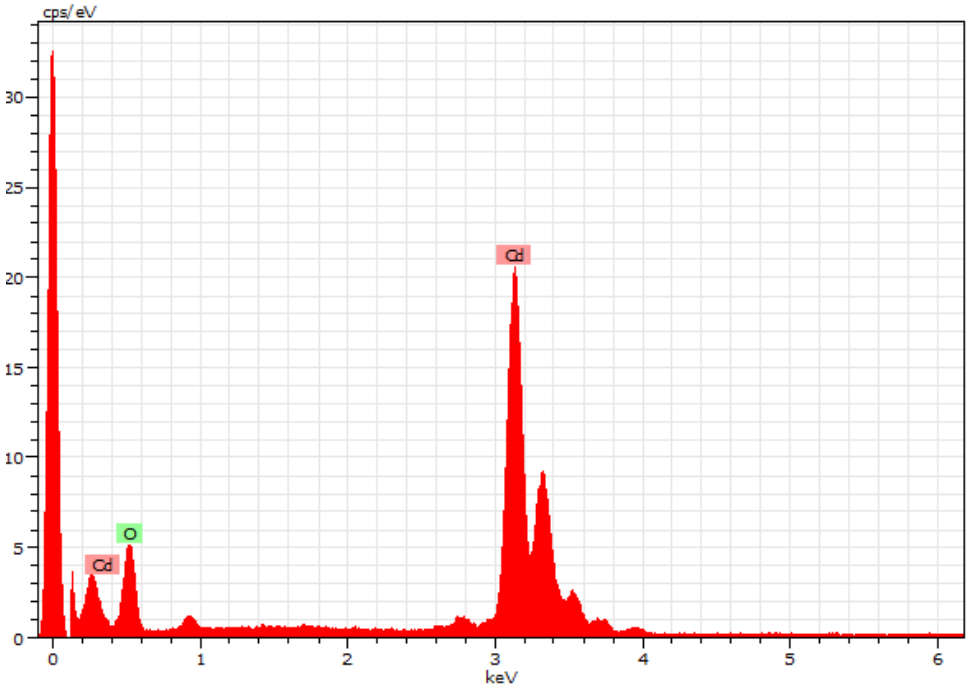

Figure 4(a) Energy dispersive spectrum of (a) pure CdO,

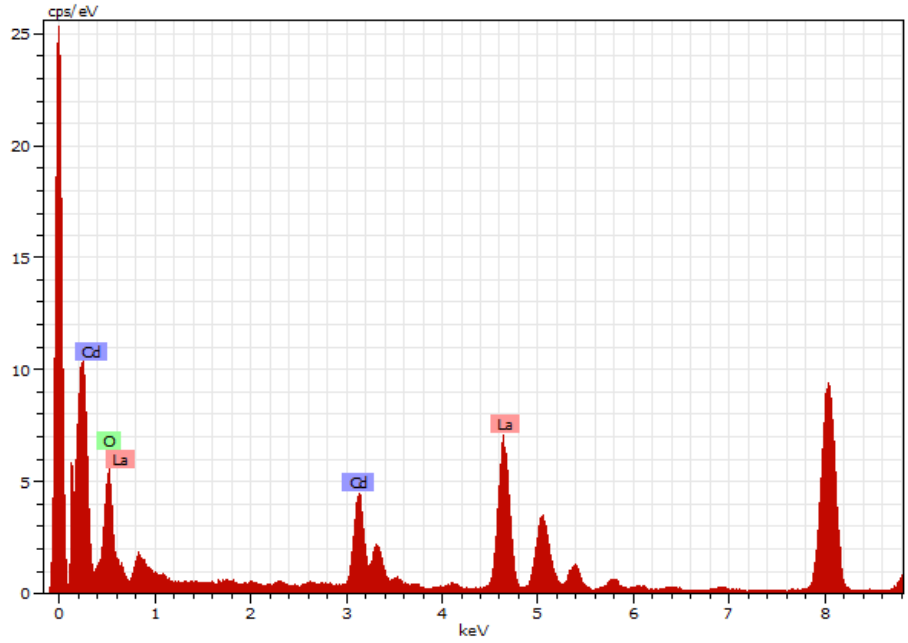

Figure 4(b) Energy dispersive spectrum of (b) CdO/ La_2O_3

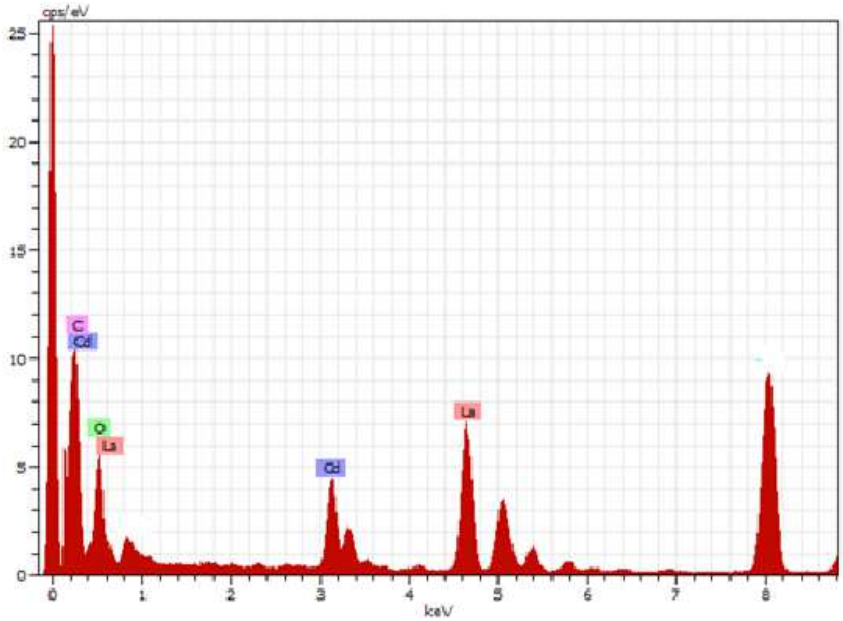

Figure 4(c) Energy dispersive spectrum of (c) CdO/ La_2O_3/ PVP nanocomposites

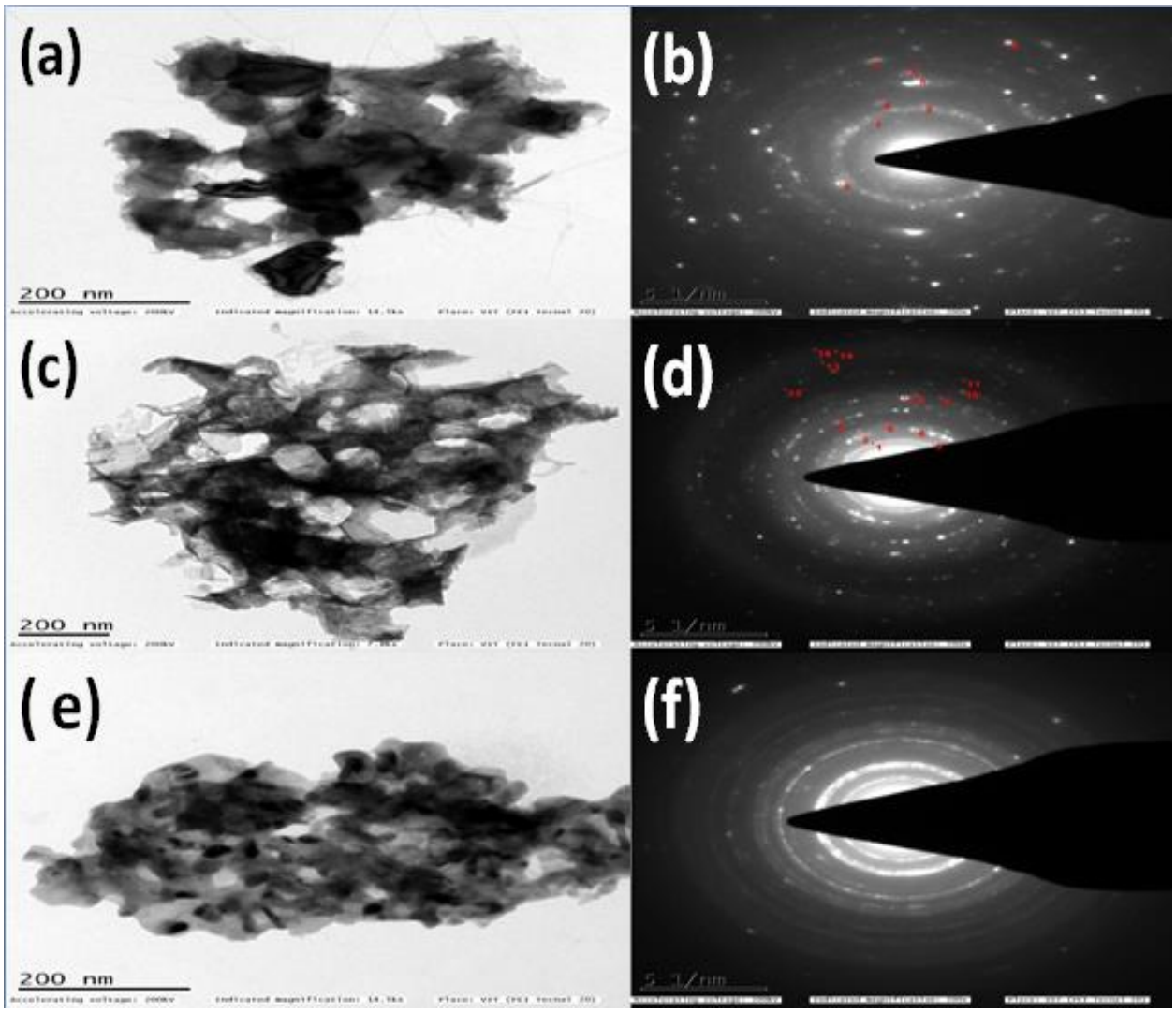

Figure 5(a-f) TEM and SAED images of pure CdO (a&b), CdO/ La_2O_3 (c & d) and CdO/ La_2O_3/ PVP (e& f) nanocomposites

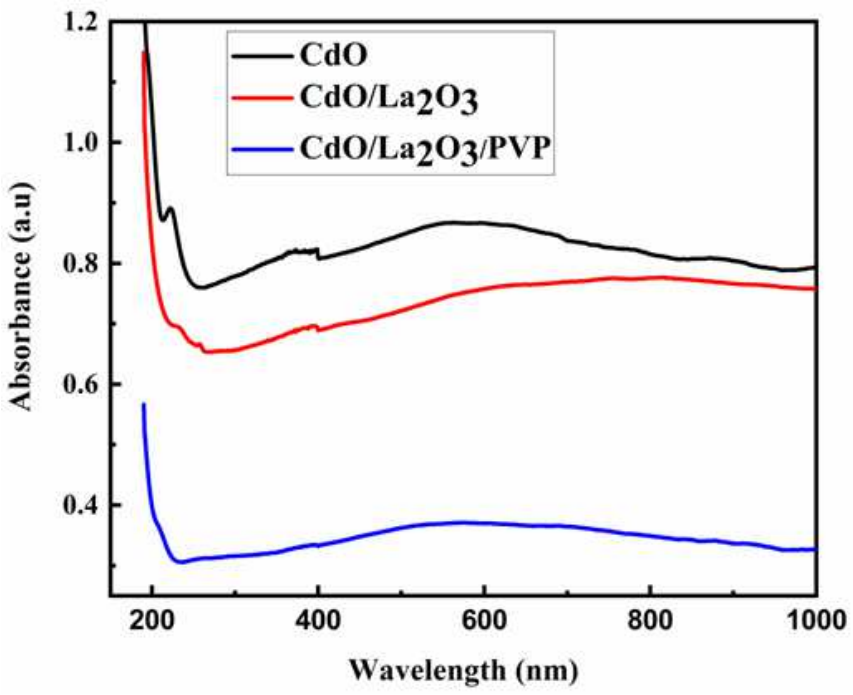

Figure 6 **UV-Vis absorption spectra of pure CdO, CdO/ La_2O_3 and CdO/ La_2O_3/ PVP nanocomposites**

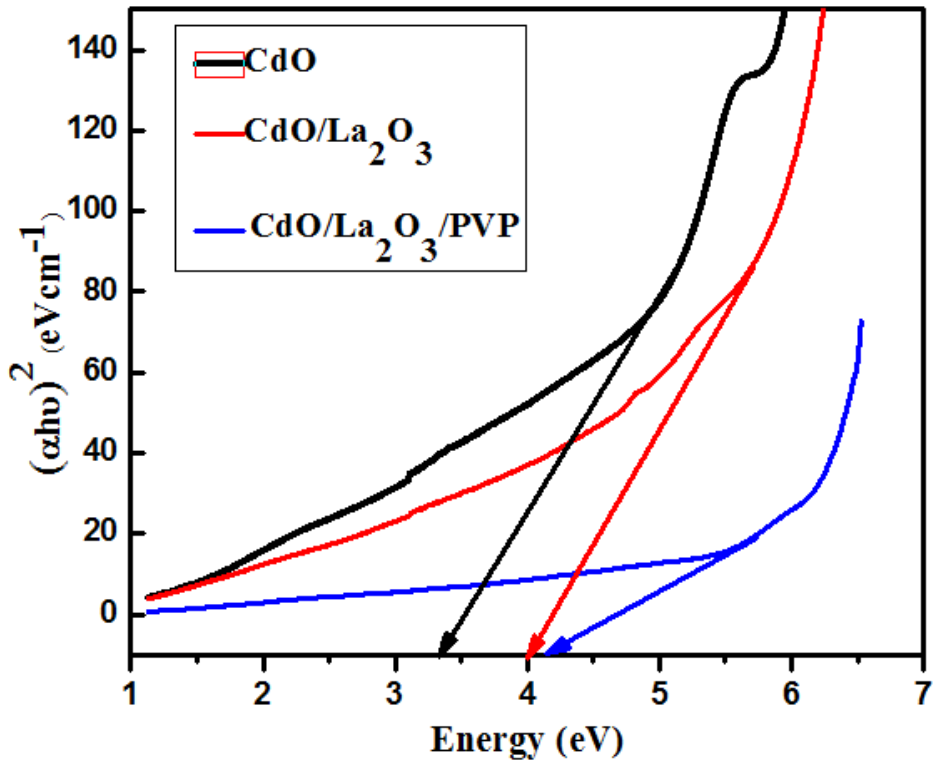

Figure7 **Band gap spectra of pure CdO, CdO/La_2O_3 and CdO/La_2O_3/ PVP nanocomposites**

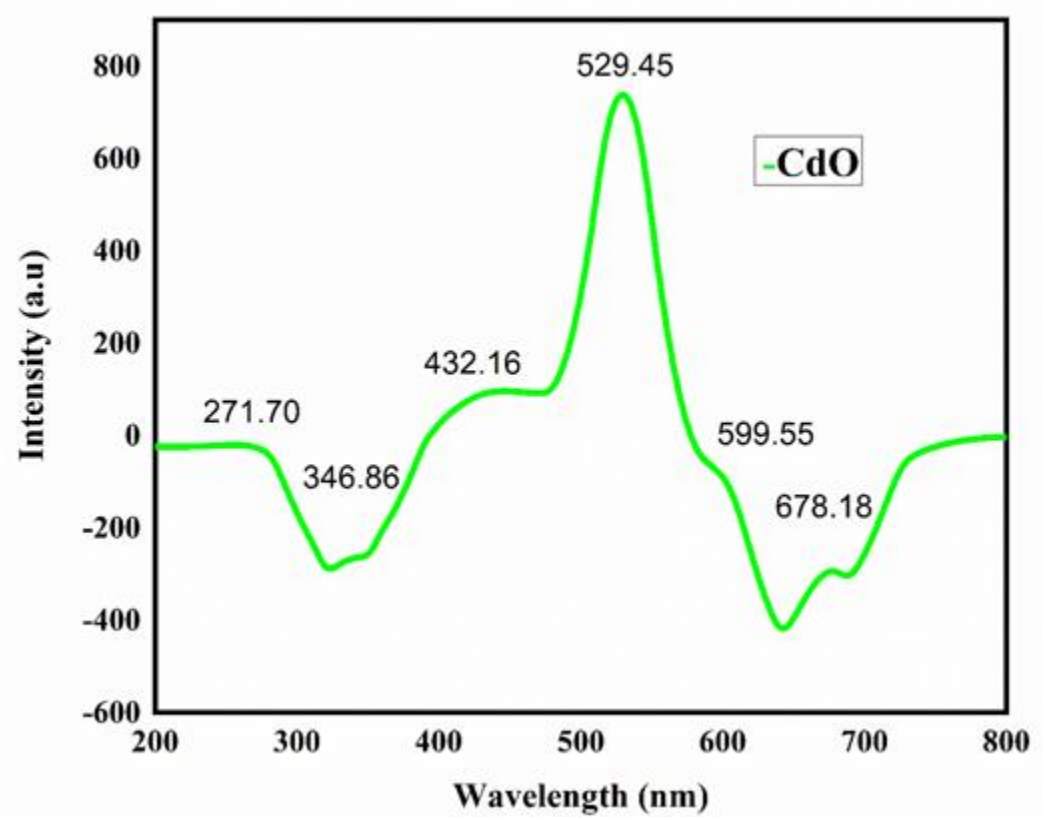

Figure 8(a) PL spectra of pure CdO nanoparticles

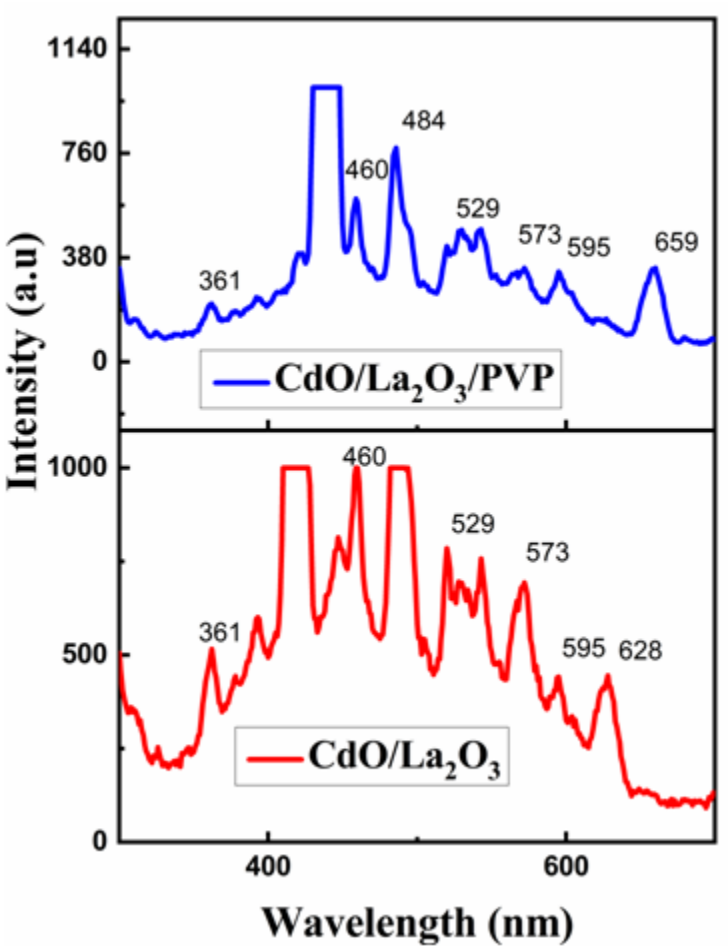

Figure 8(b) PL spectra of CdO/La_2O_3 and CdO/La_2O_3/ PVP nanocomposites

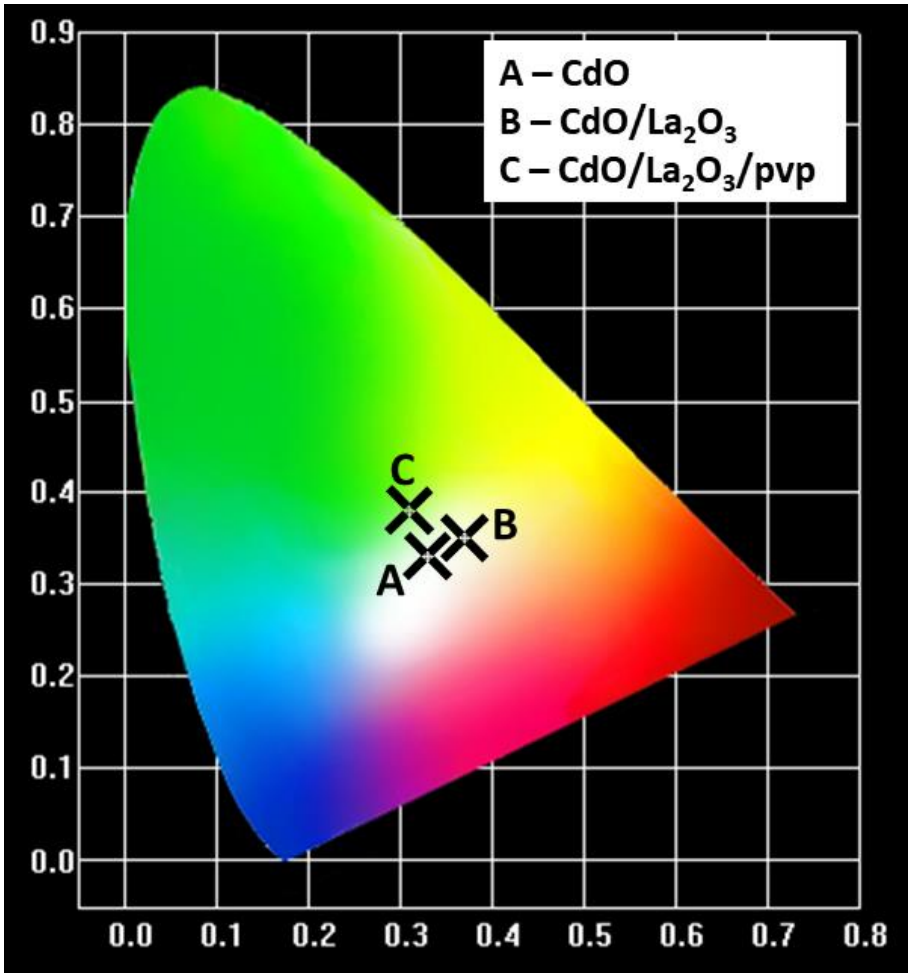

Figure 8 (c) CIE chromaticity diagram of CdO, CdO/ La_2O_3 and CdO/ La_2O_3/PVP nanocomposites

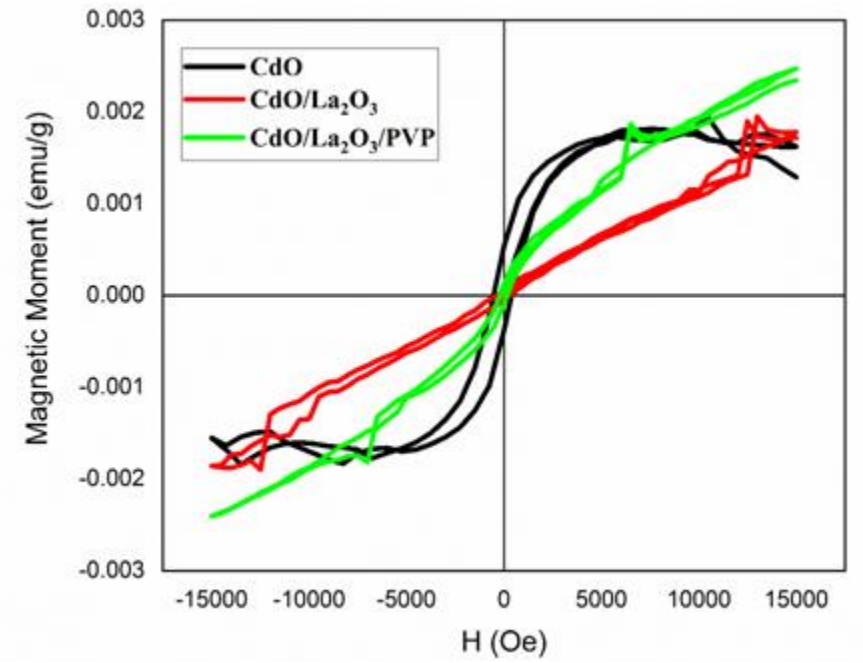

Figure 9 **Magnetization hysteresis (M-H) curves of pure CdO, CdO/La_2O_3 and CdO/La_2O_3/ PVP nanocomposites**

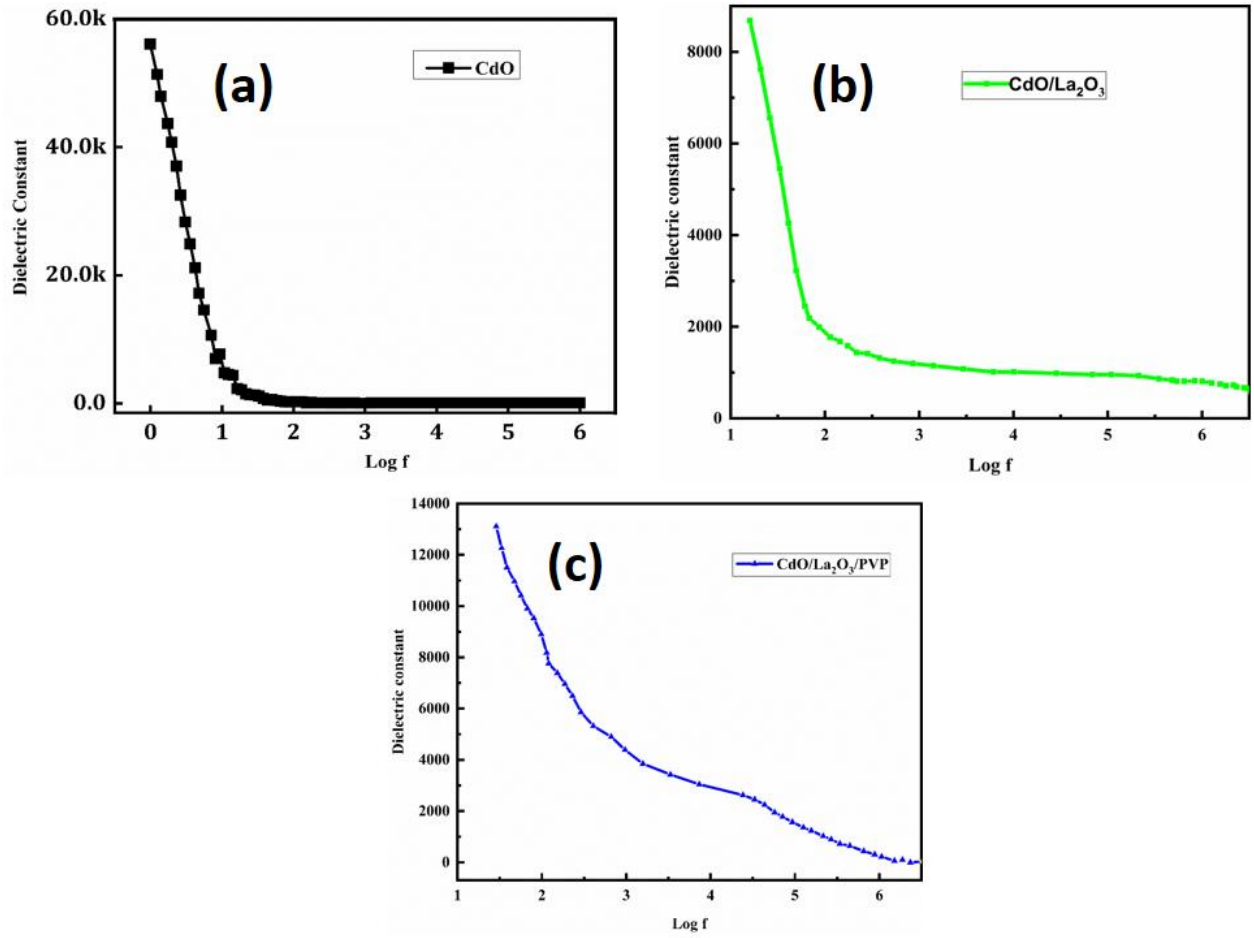

Figure 10 (a-c) Dielectric constant for pure CdO, CdO/La_2O_3 and CdO/La_2O_3/ PVP nanocomposite at room temperature

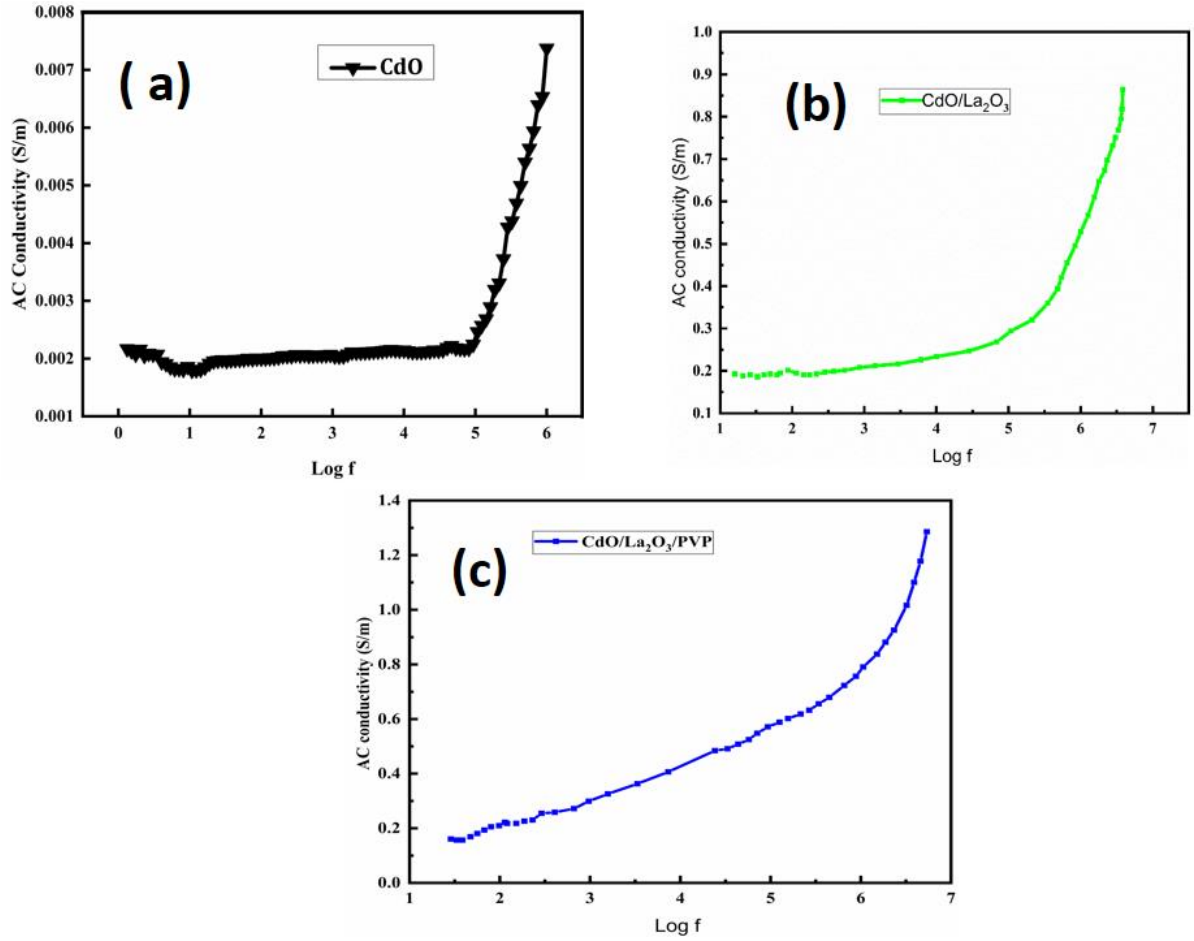

Figure 11 (a-c) Electrical conductivity with frequency of CdO, CdO/La_2O_3 and CdO/La_2O_3/PVP nanocomposite at room temperature.

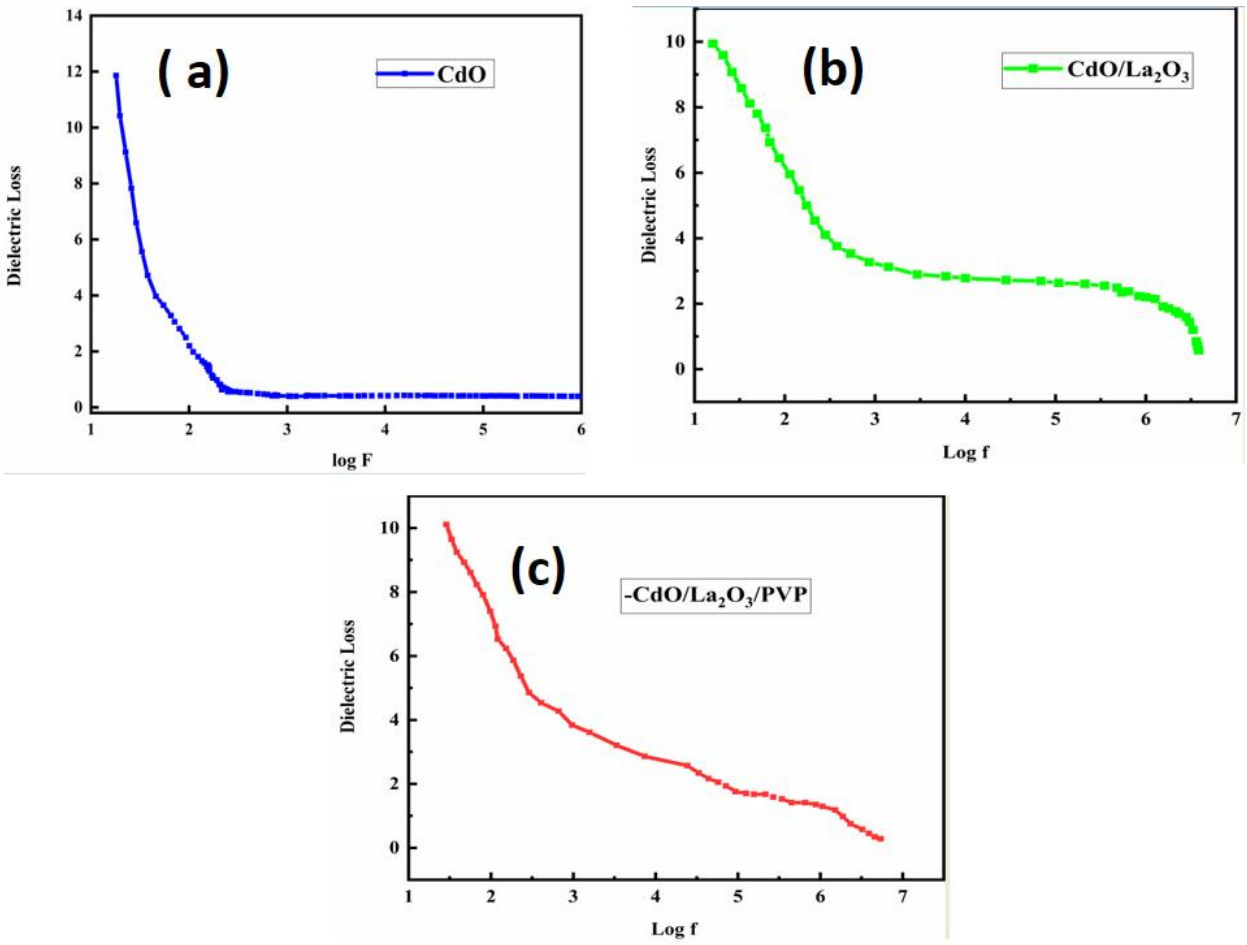

Figure 12 (a-c) Dielectric loss of CdO, CdO/ La_2O_3 and CdO/ La_2O_3/ PVP nanocomposite

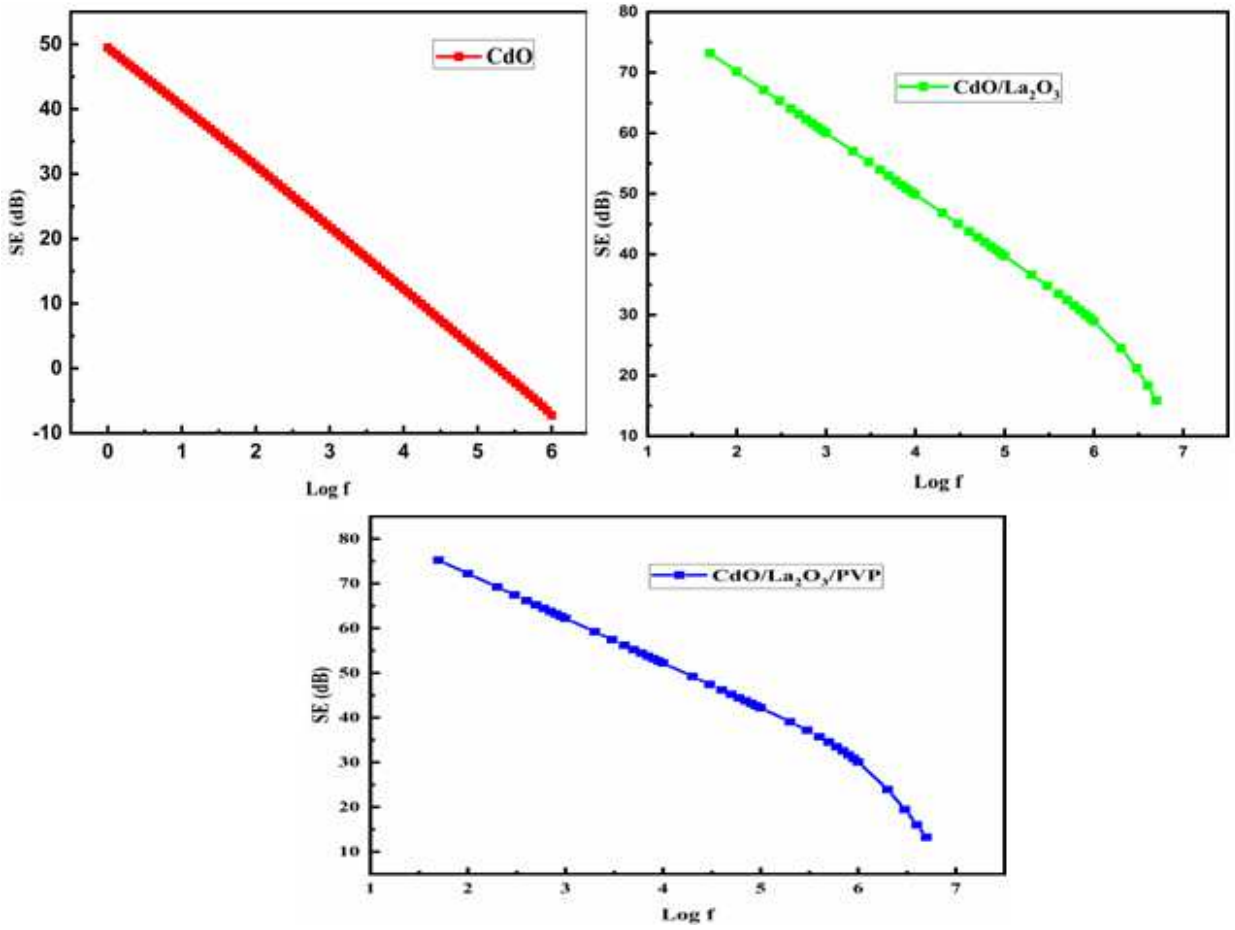

Figure 13 **EMI shielding Effectiveness of CdO, CdO/$La_2O_3$and CdO/La_2O_3/ PVP nanocomposite**

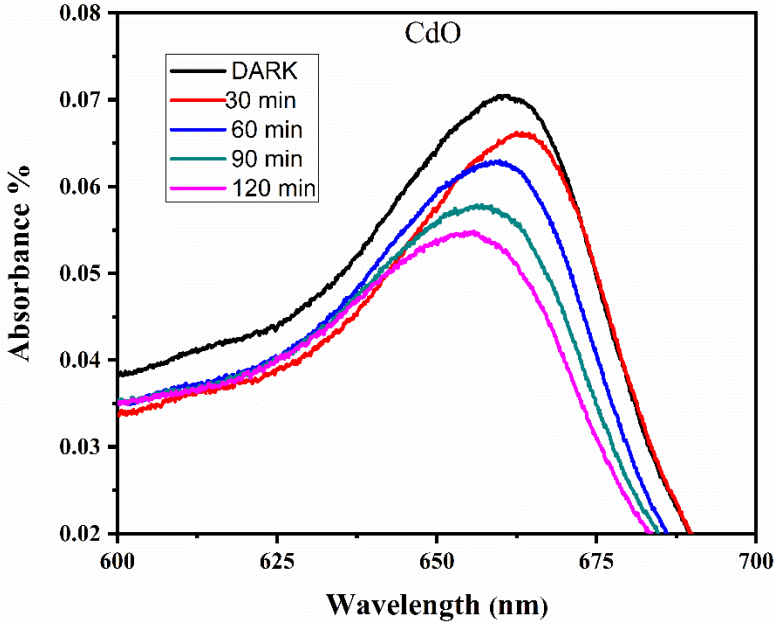

Figure 14 (a) Time dependent absorbance spectra pure CdO.

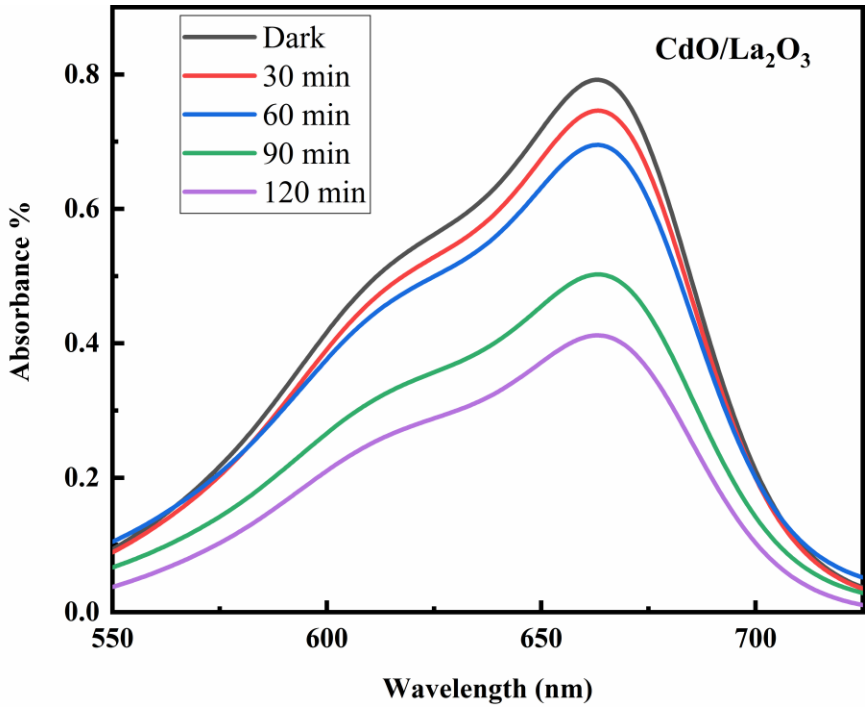

Figure 14 (b) Time dependent absorbance spectra. CdO/La_2O_3 nanocomposites

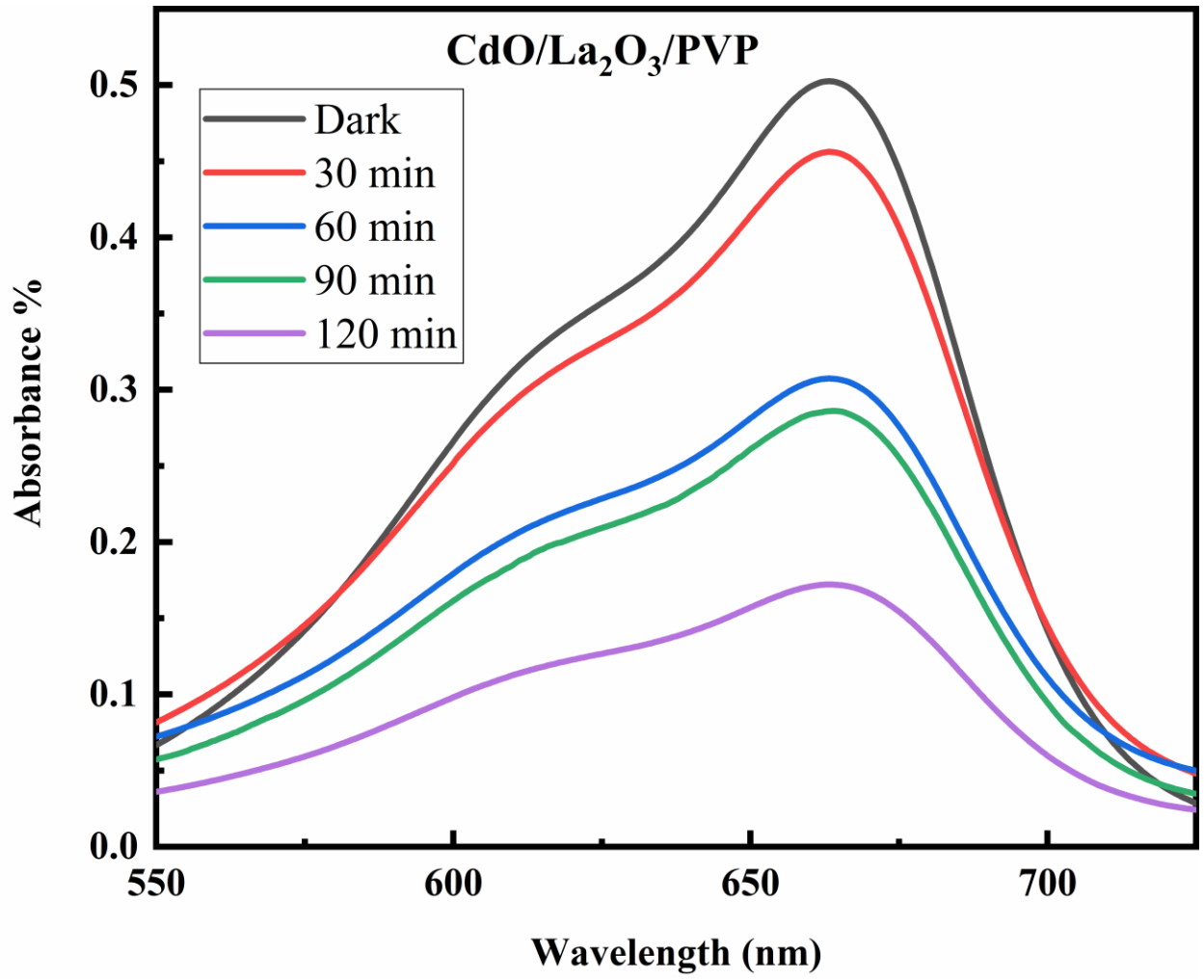

Figure 14 (c) Time dependent absorbance spectra CdO/La_2O_3/ PVP nanocomposites

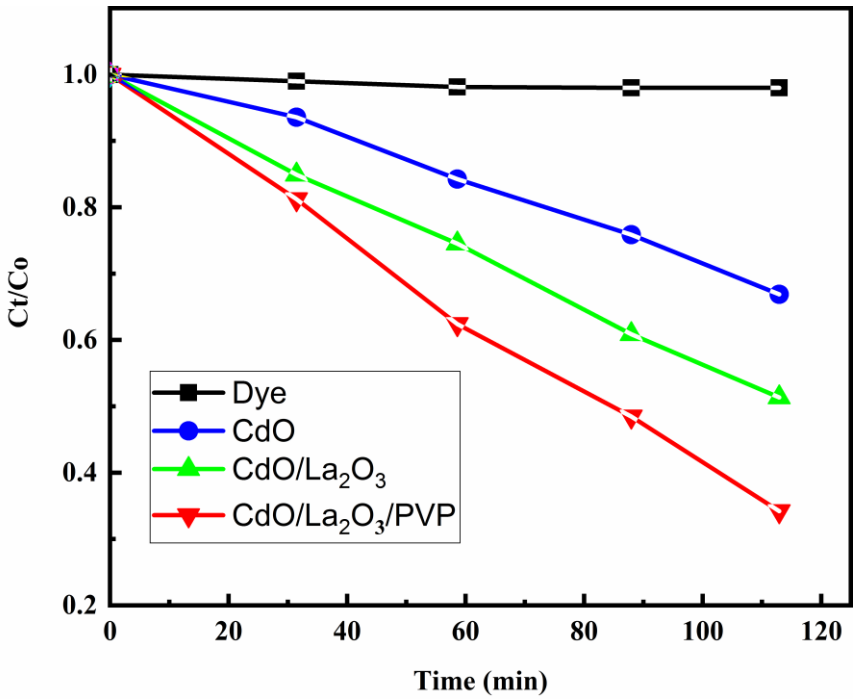

Figure 15 (a) Photocatalytic degradation analysis curves of pure CdO , CdO/ La_2O_3 and CdO/ La_2O_3/ PVP nanocomposites

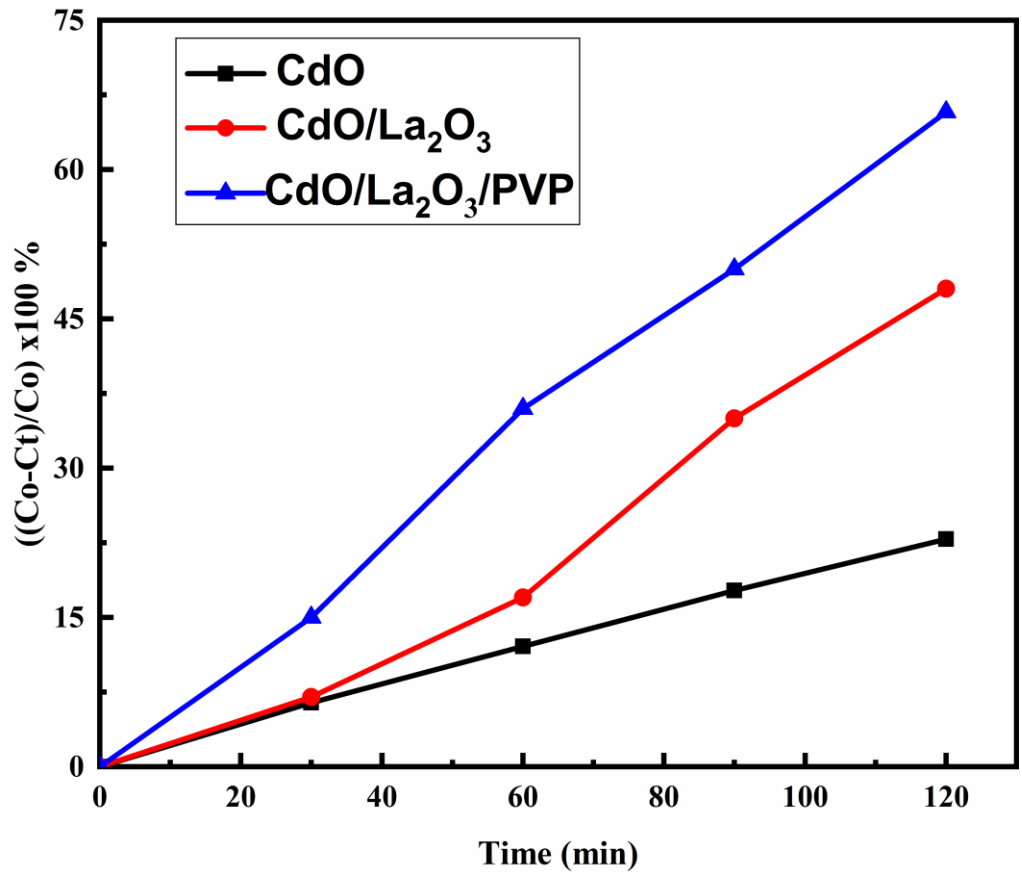

Figure 15 (b) Photocatalytic degradation efficiency analysis curves of pure CdO CdO/ $La_2O_3$and CdO/ La_2O_3/PVP Nanocomposites

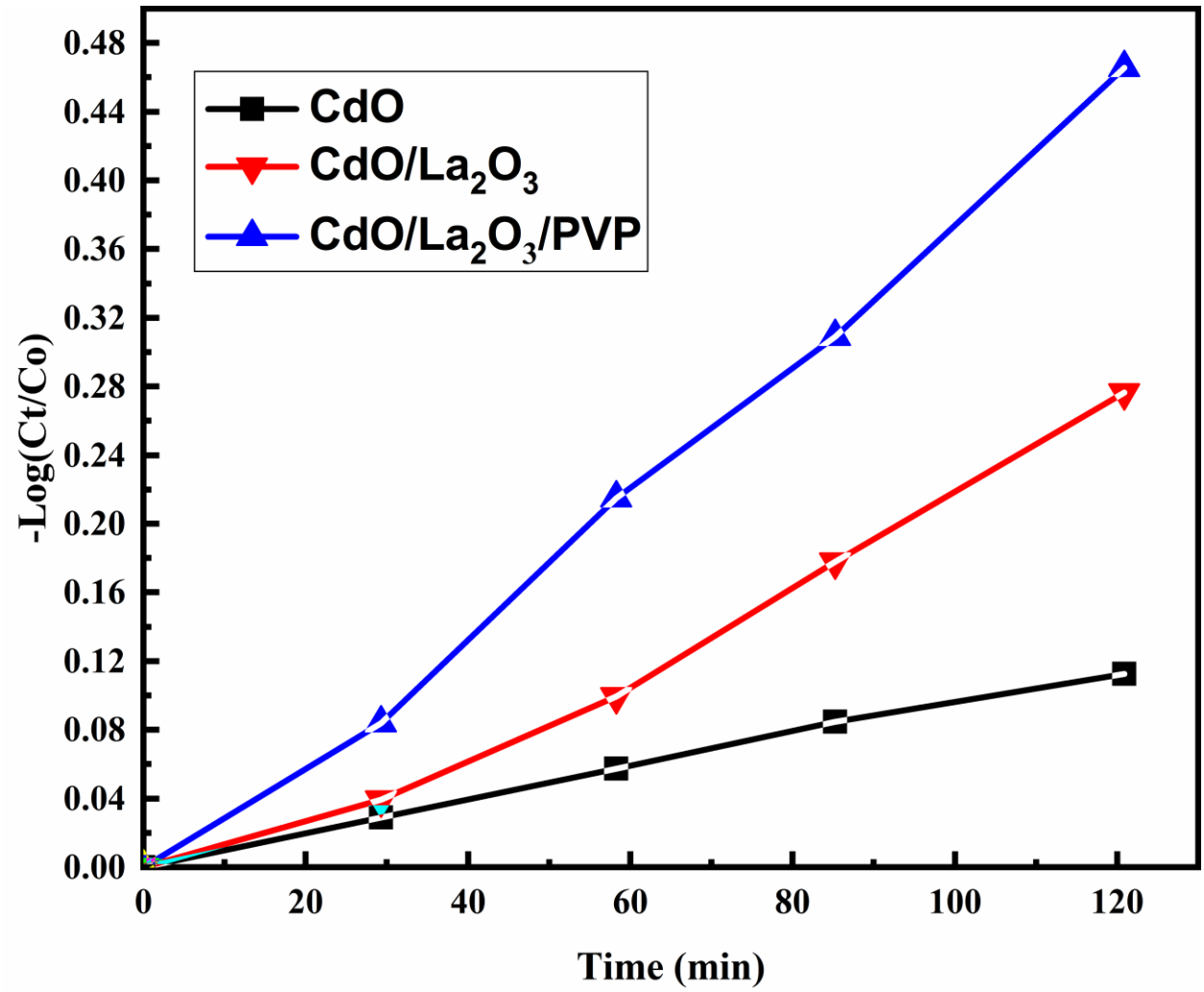

Figure15 (c) Kinetic curve study of photocatalytic degrdation of MB dye in pure CdO. CdO/ La_2O_3 and CdO/ La_2O_3/ PVP nanocomposites

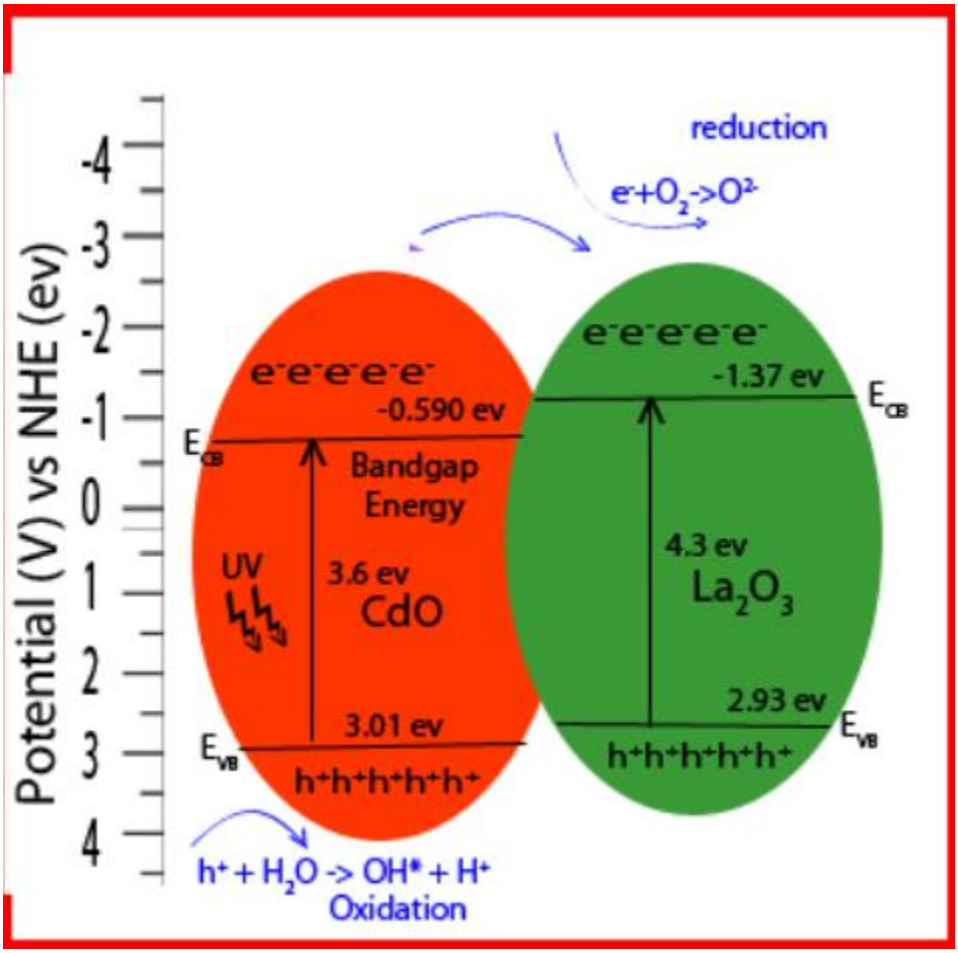

Figure16 **The schematic representation of photocatalytic mechanism of CdO, CdO/ La_2O_3 and CdO/ La_2O_3/ PVP nanocomposite**

Figures

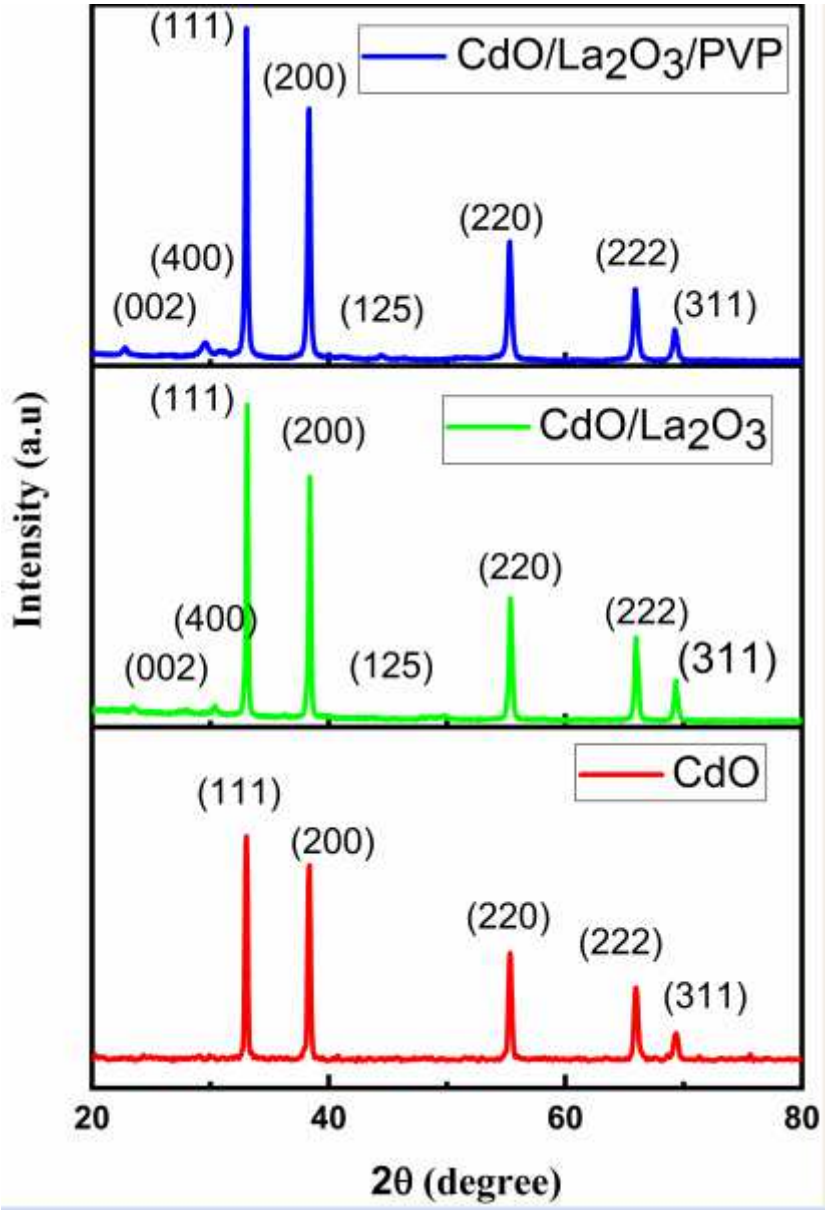

Figure 1

XRD patterns of pure CdO, CdO/La2O3 and CdO/La2O3/ PVP nanocomposites

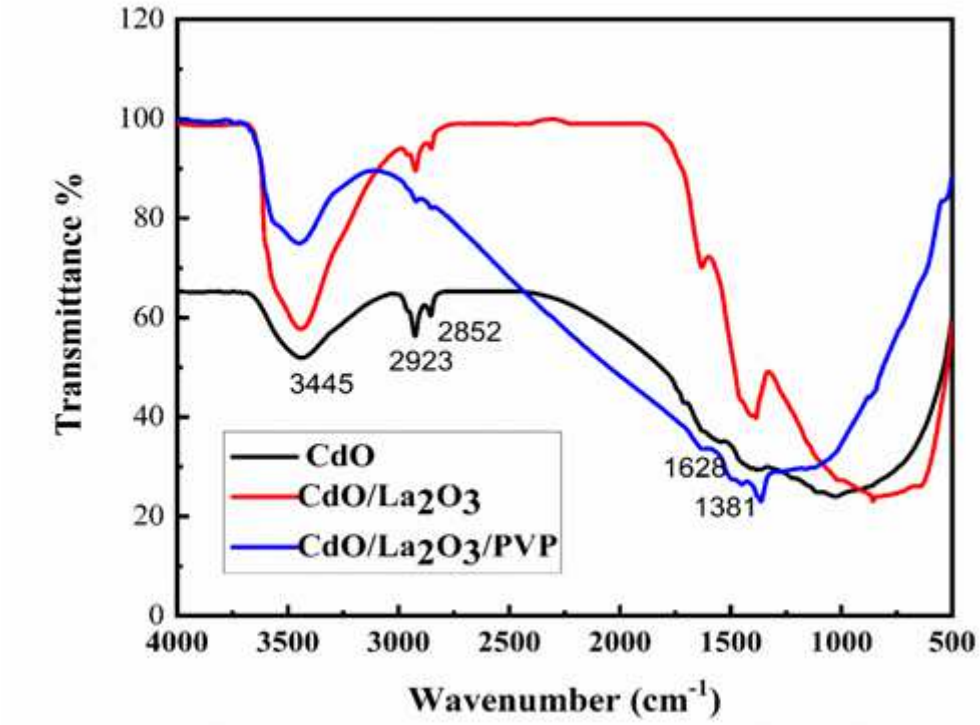

Figure 2

FTIR spectra of pure CdO, CdO/La2O3 and CdO/La2O3/PVP nanocomposites.

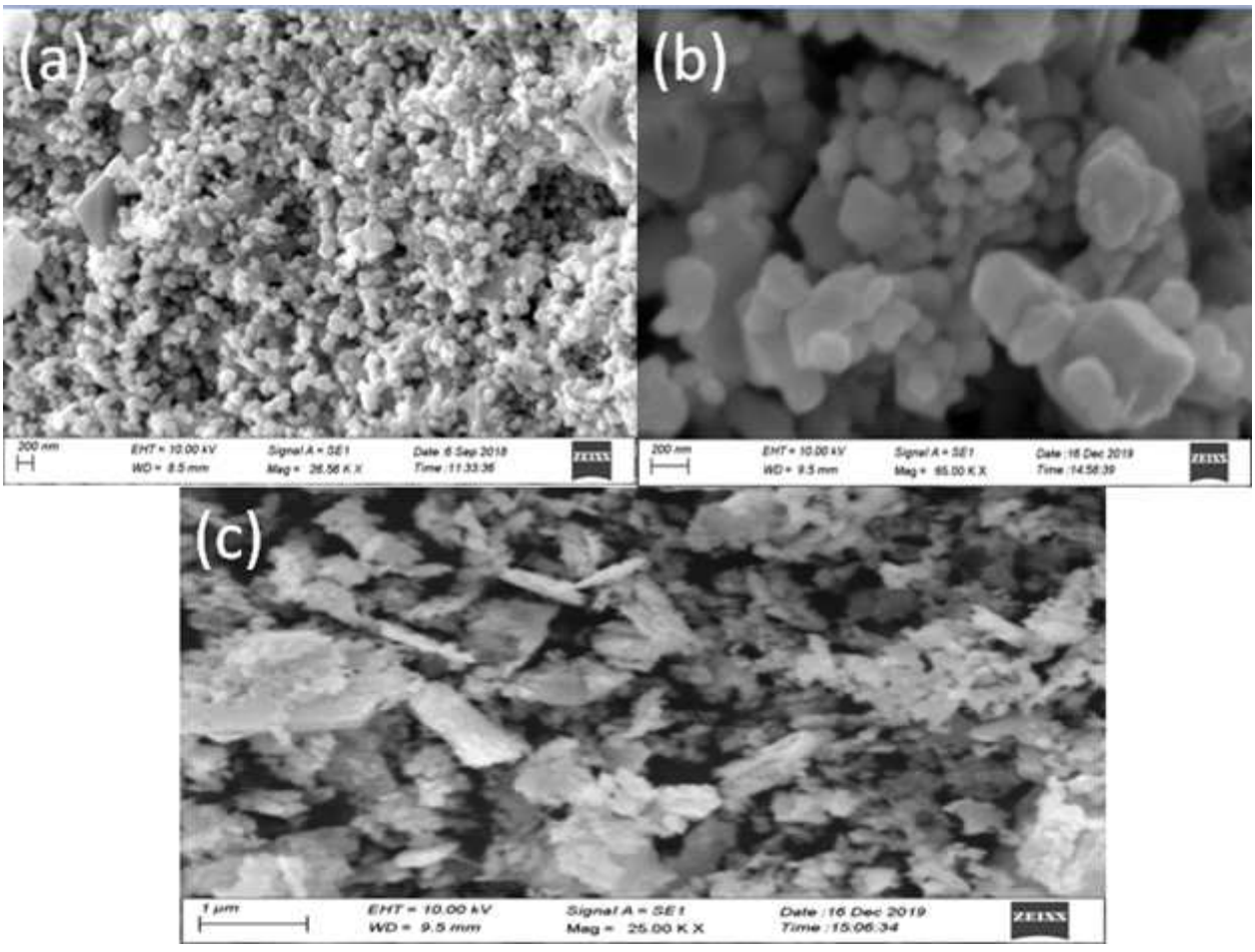

Figure 3

Scanning electron micrographs of (a) pure CdO, (b) CdO/La2O3 and (c) CdO/La2O3/PVP nanocomposites

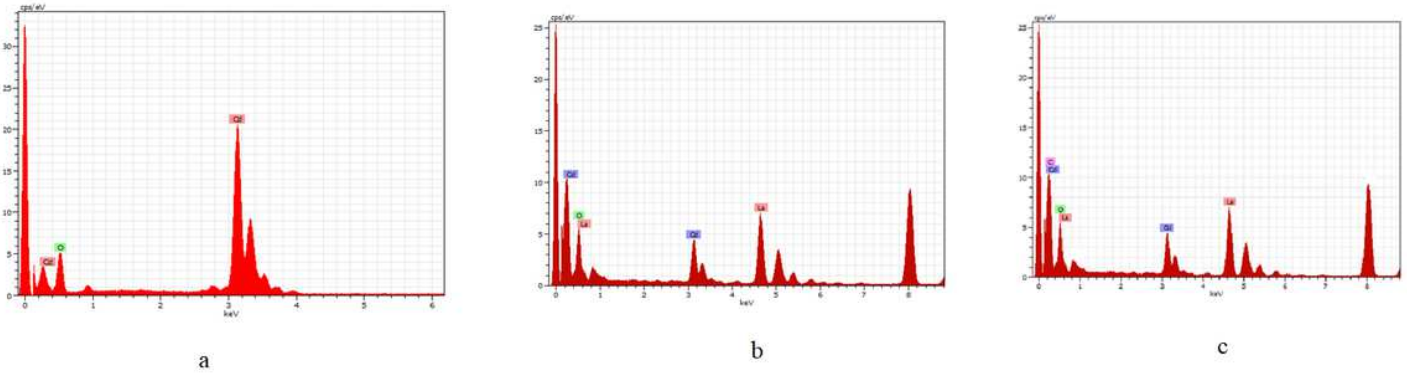

Figure 4

Energy dispersive spectra of (a) pure CdO, (b) CdO/La2O3 and (c) CdO/La2O3/ PVP nanocomposites.

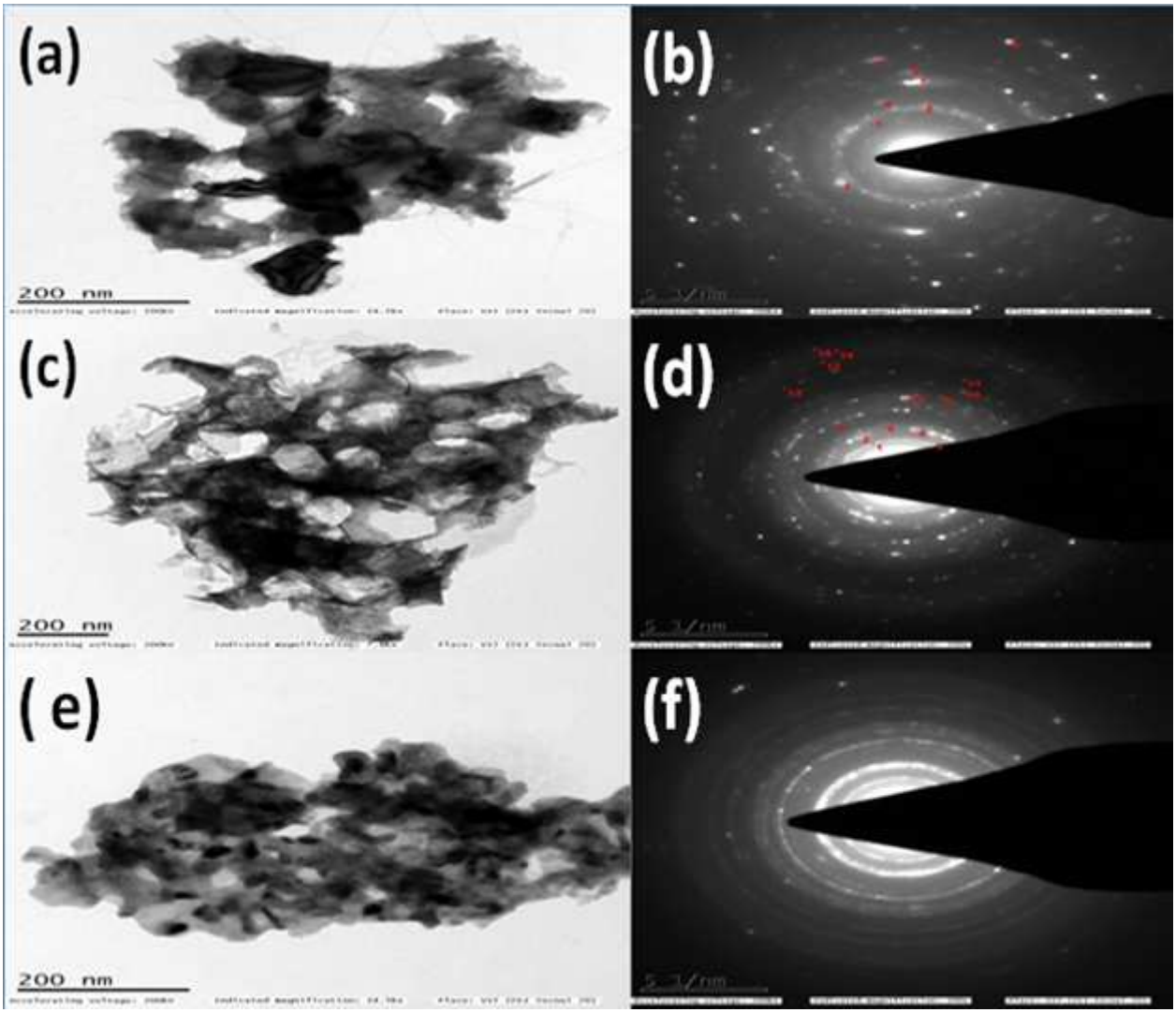

Figure 5

TEM and SAED images of pure CdO (a&b), CdO/La2O3 (c & d) and CdO/La2O3/ PVP (e&f) nanocomposites

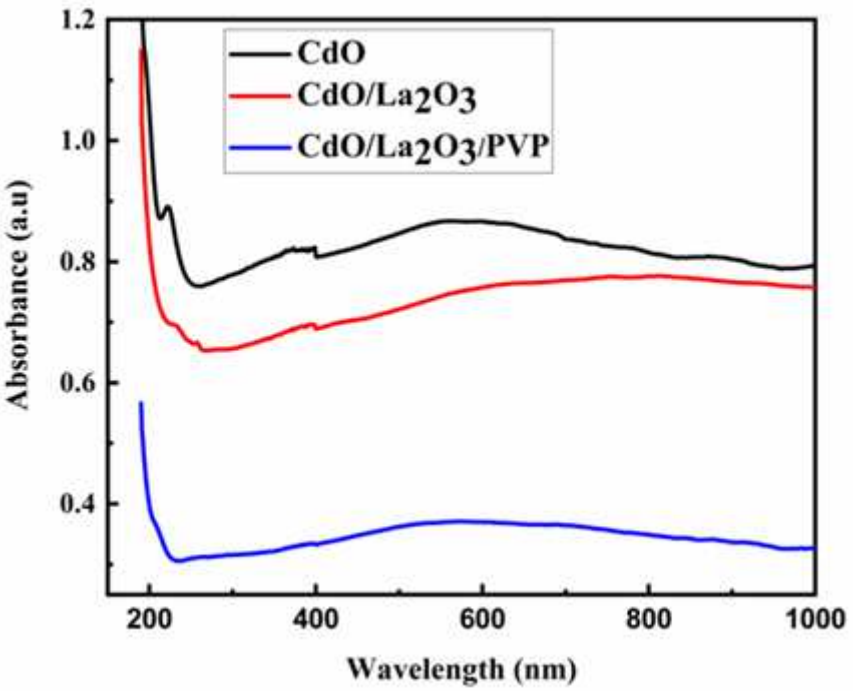

Figure 6

UV-Vis absorption spectra of pure CdO, CdO/La2O3 and CdO/La2O3/ PVP nanocomposites

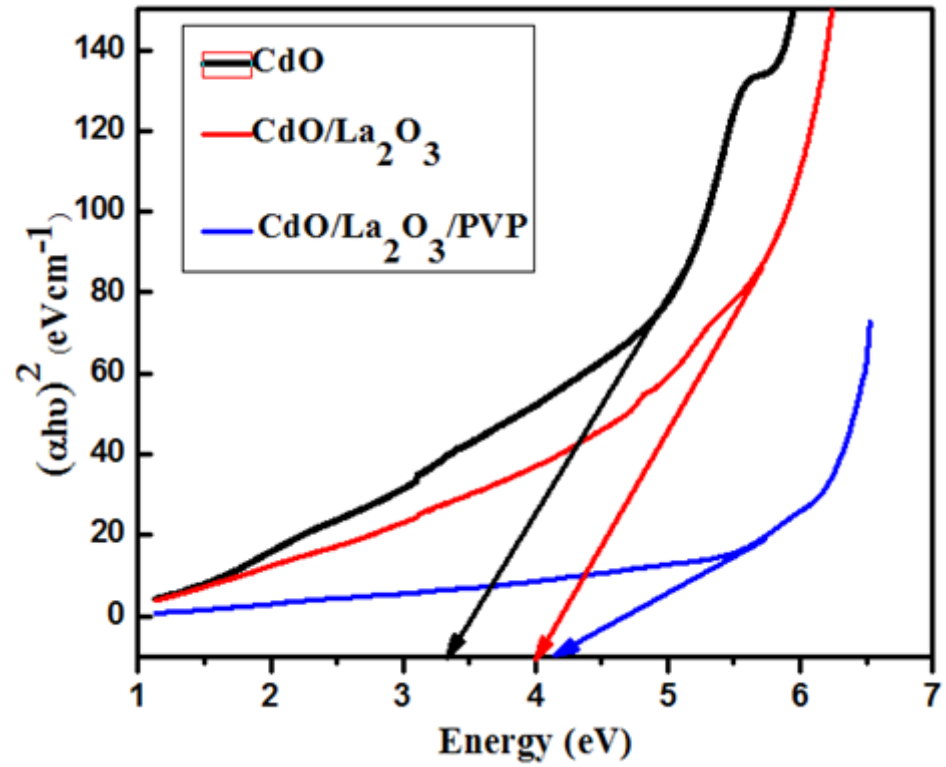

Figure 7

Band gap spectra of pure CdO, CdO/La2O3 and CdO/La2O3/ PVP nanocomposites .

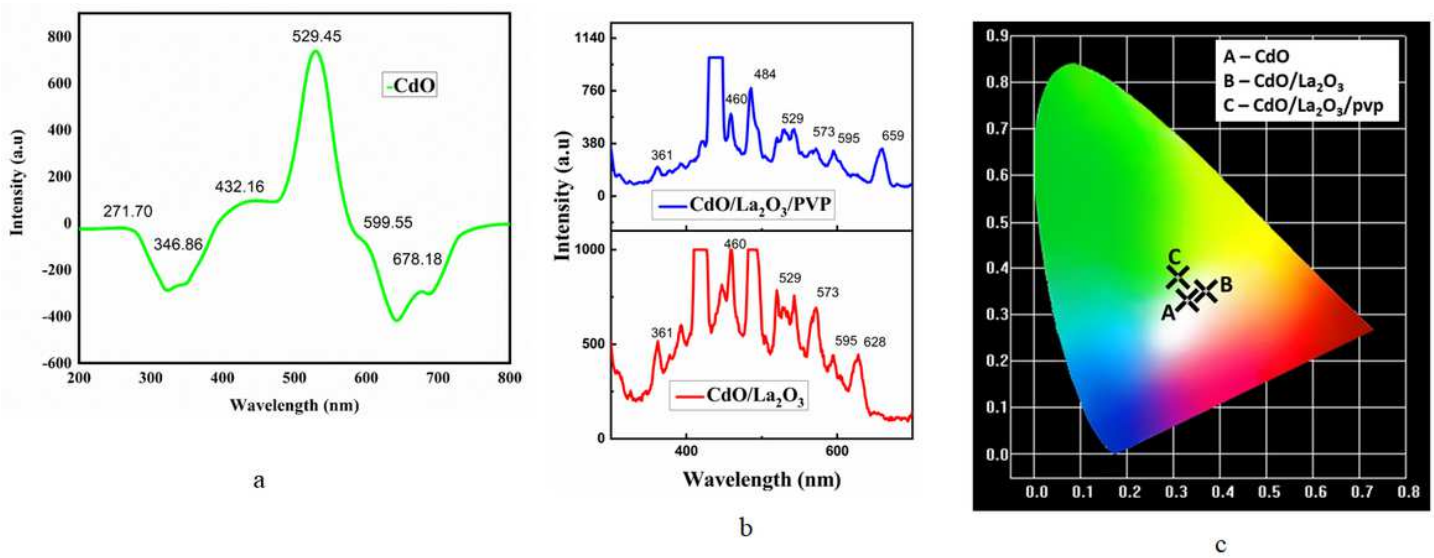

Figure 8

(a) PL spectra of pure CdO nanoparticles (b) PL spectra of CdO/La2O3 and CdO/La2O3/ PVP nanocomposites (c) CIE chromaticity diagram of CdO, CdO/La2O3 and CdO/La2O3/PVP nanocomposites

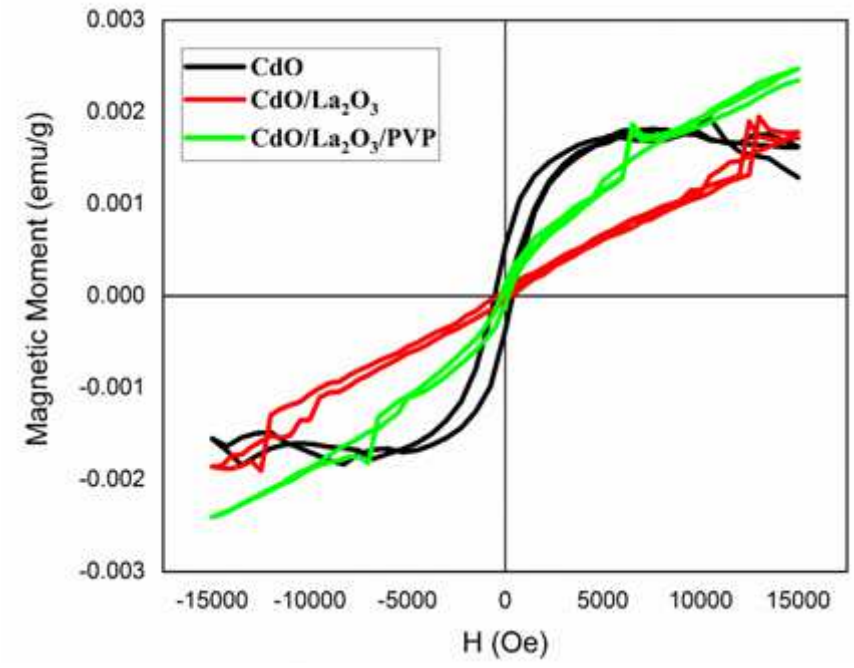

Figure 9

Magnetization hysteresis (M-H) curves of pure CdO, CdO/La2O3 and CdO/La2O3/PVP nanocomposites

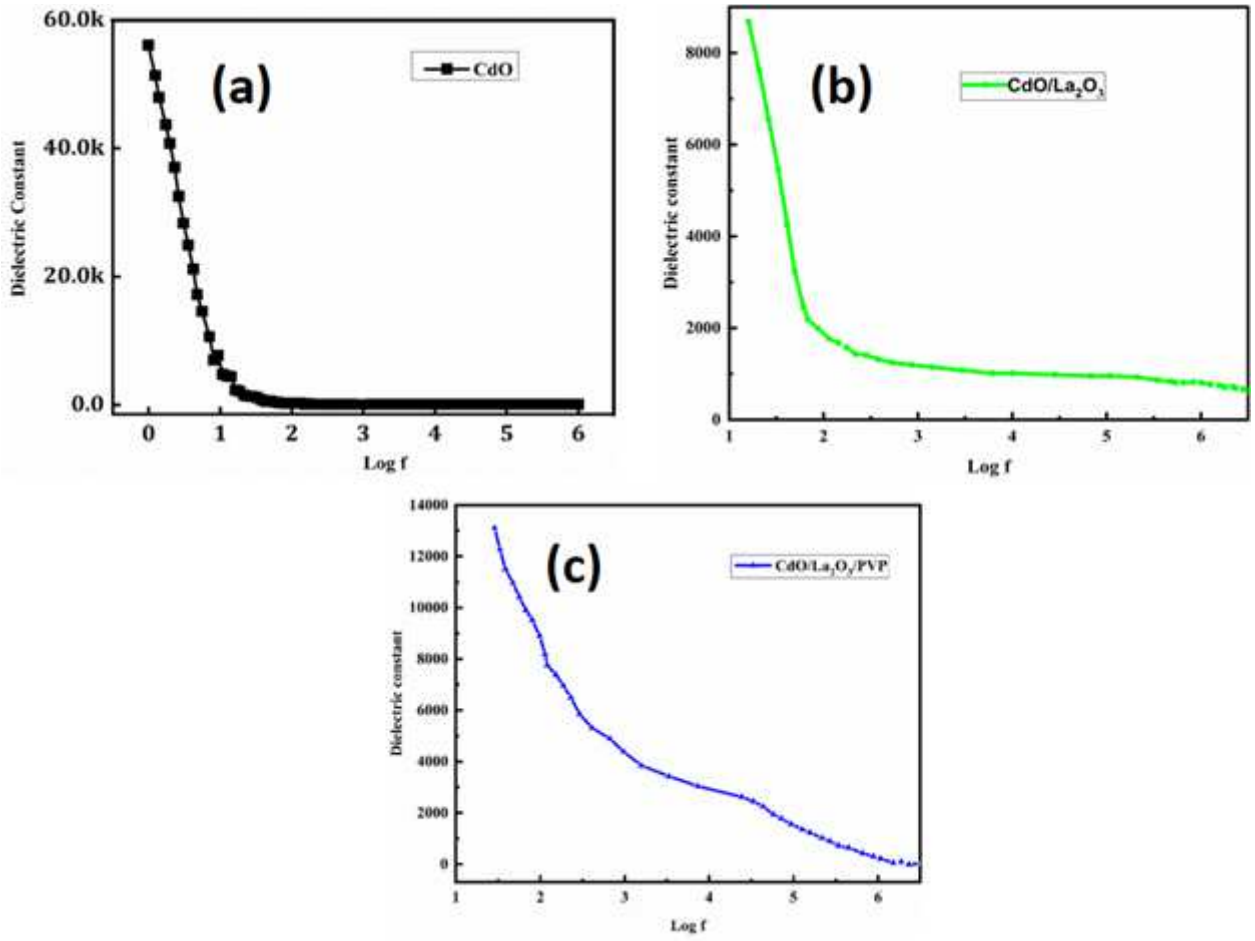

Figure 10

Dielectric constant for pure CdO, CdO/La2O3 and CdO/La2O3/PVP nanocomposite at room temperature

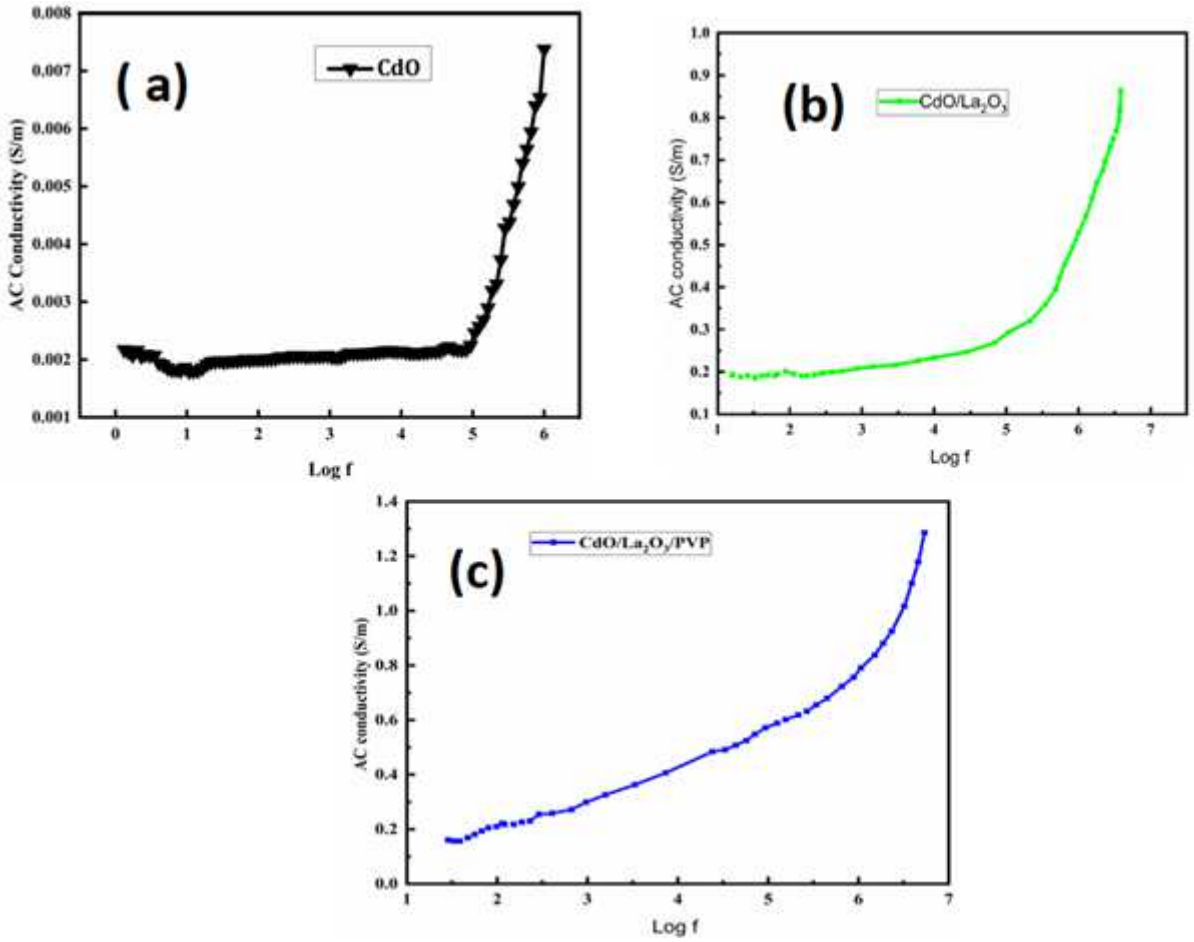

Figure 11

Electrical conductivity with frequency of CdO, CdO/La2O3 and CdO/La2O3/ PVP nanocomposite at room temperature.

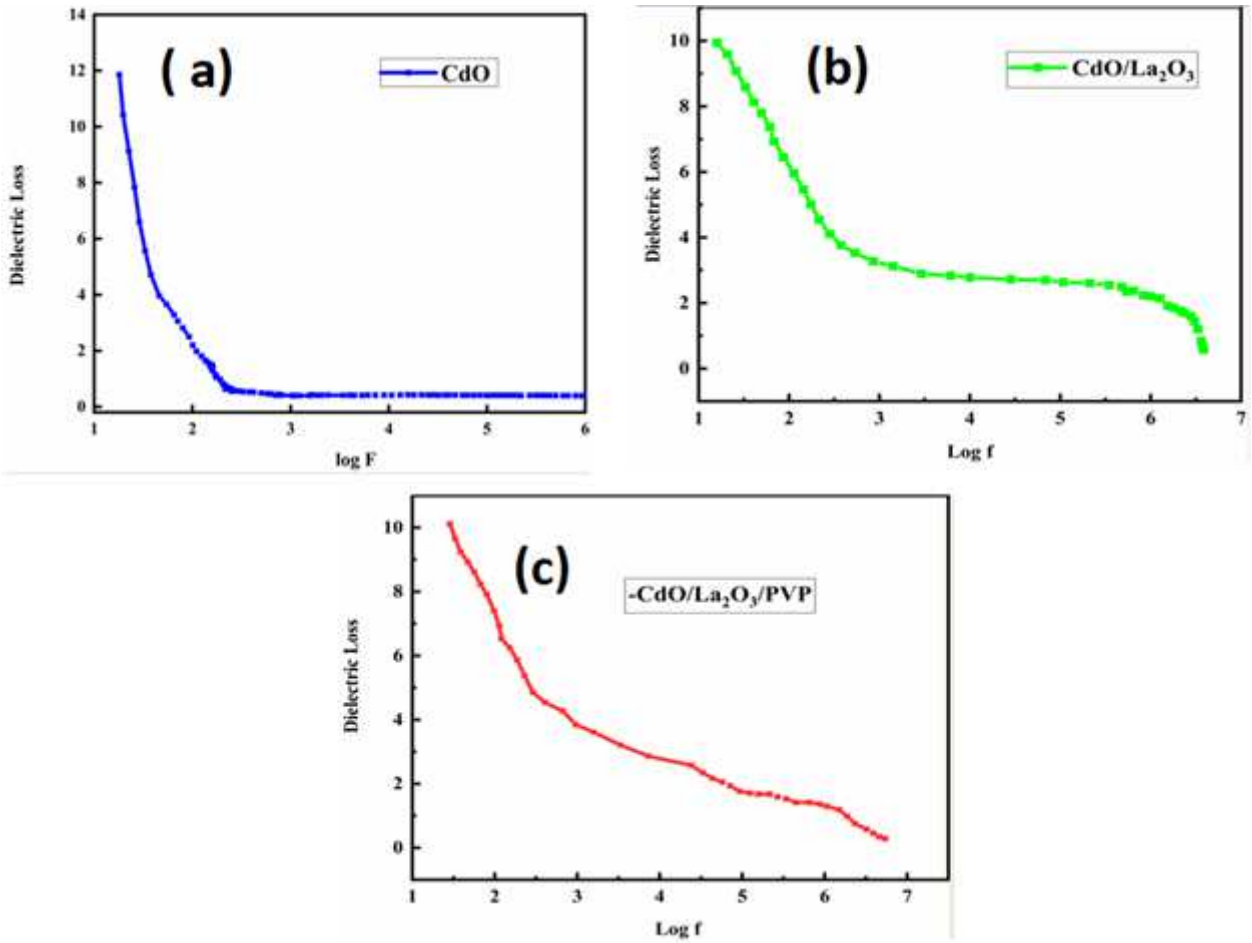

Figure 12

Dielectric loss of CdO, CdO/La2O3 and CdO/La2O3/PVP nanocomposite

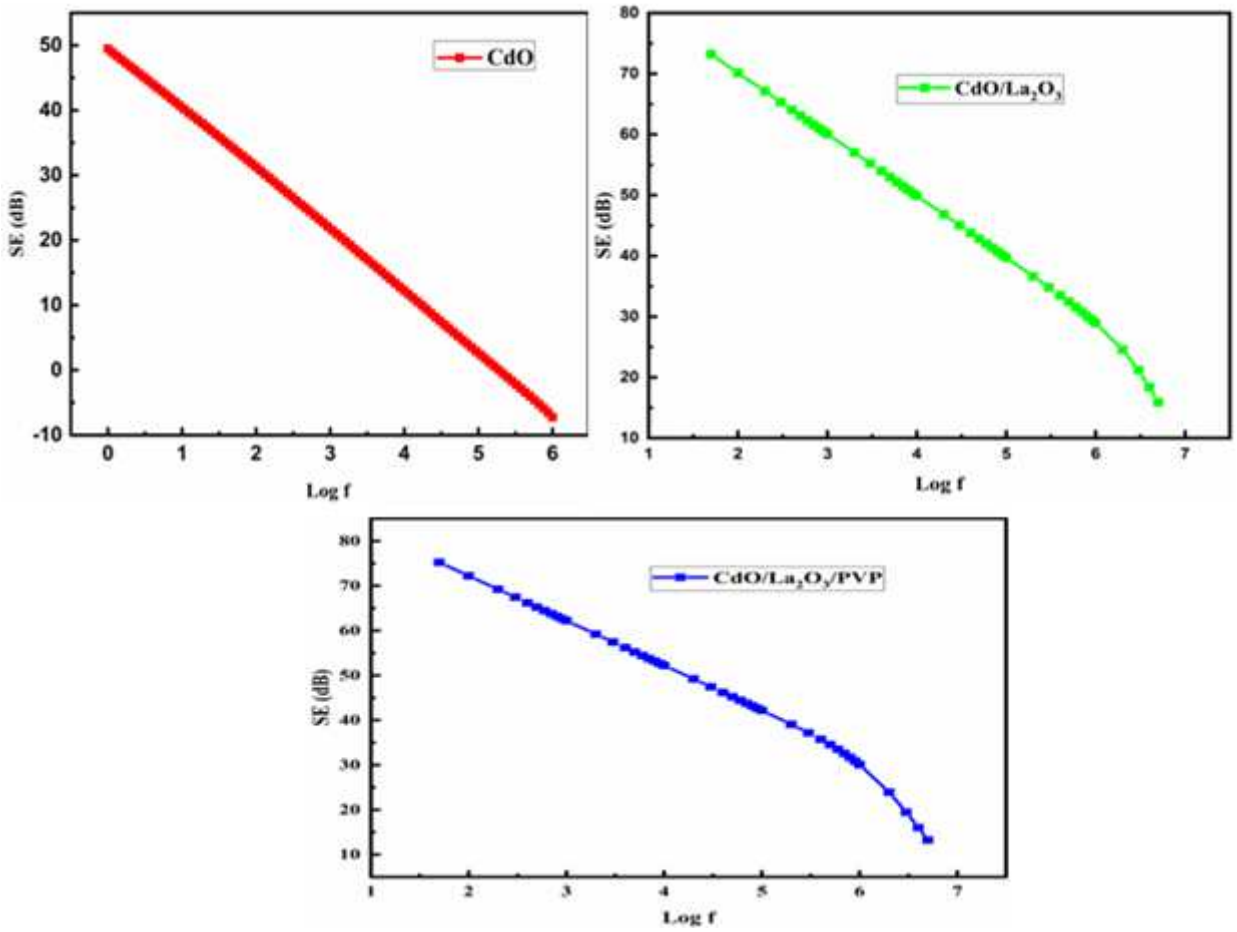

Figure 13

EMI shielding Effectiveness of CdO, CdO/La2O3 and CdO/La2O3/PVP nanocomposite

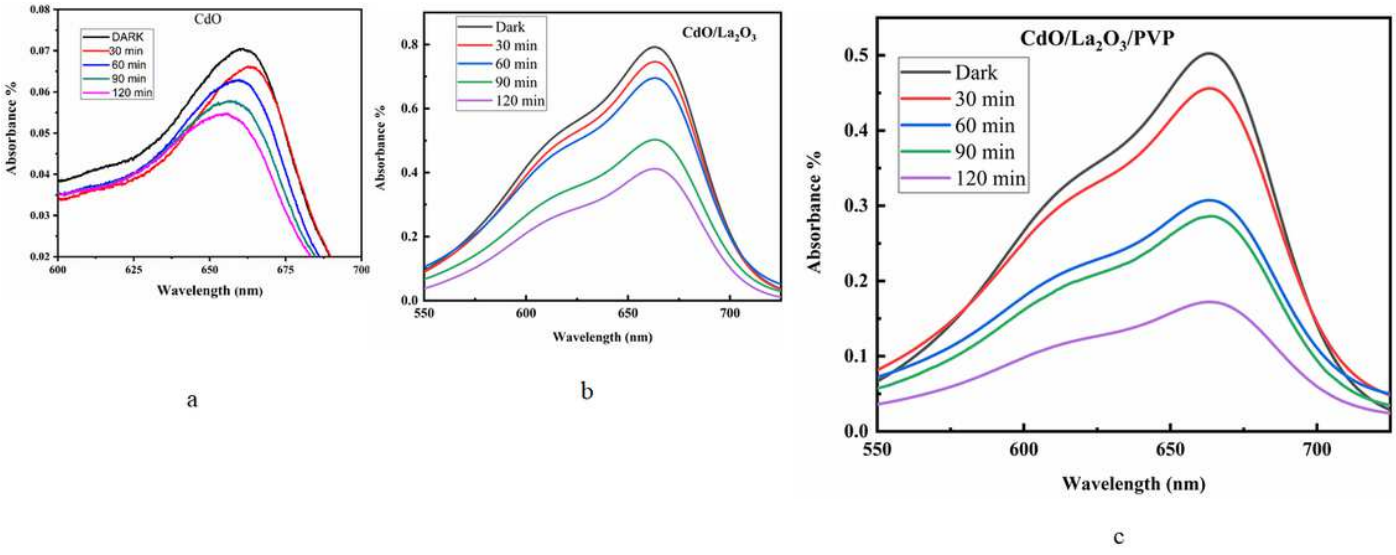

Figure 14

Time dependent absorbance spectra (a) pure CdO, (b) CdO/La2O3 and (c) CdO/La2O3/PVP nanocomposite

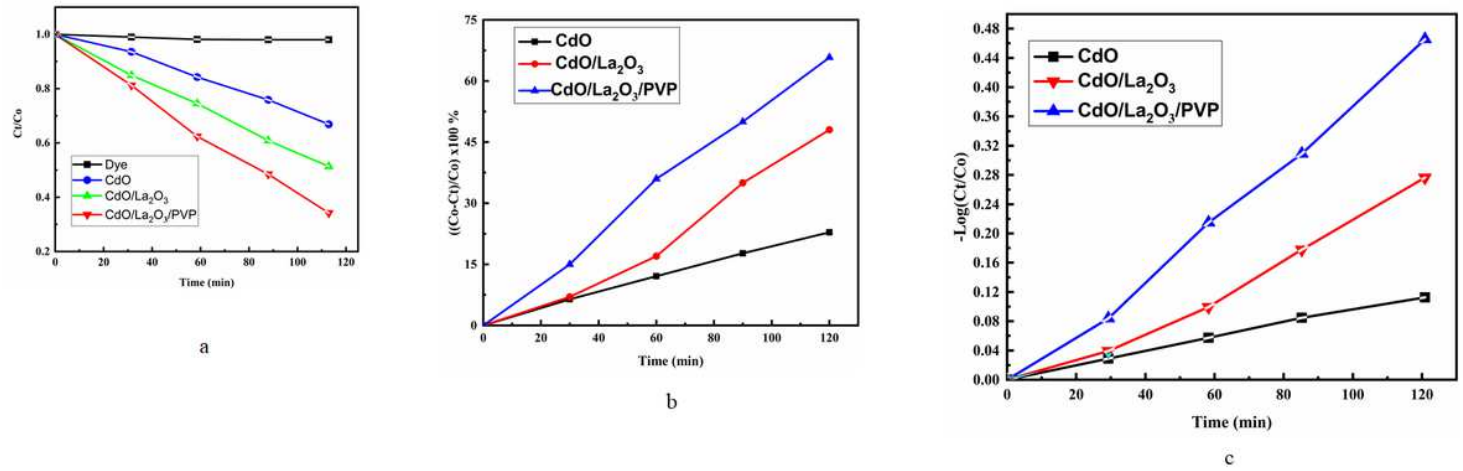

Figure 15

(a) Photocatalytic degradation analysis curves of pure CdO , CdO/La2O3 and CdO/La2O3/ PVPnanocomposites (b) Photocatalytic degradation efficiency analysis curves of pure CdO CdO/La2O3 and CdO/La2O3/PVP Nanocomposites (c) Kinetic curve study of photocatalytic degrdation of MB dye in pure CdO. CdO/La2O3 and CdO/ La2O3/PVP nanocomposites

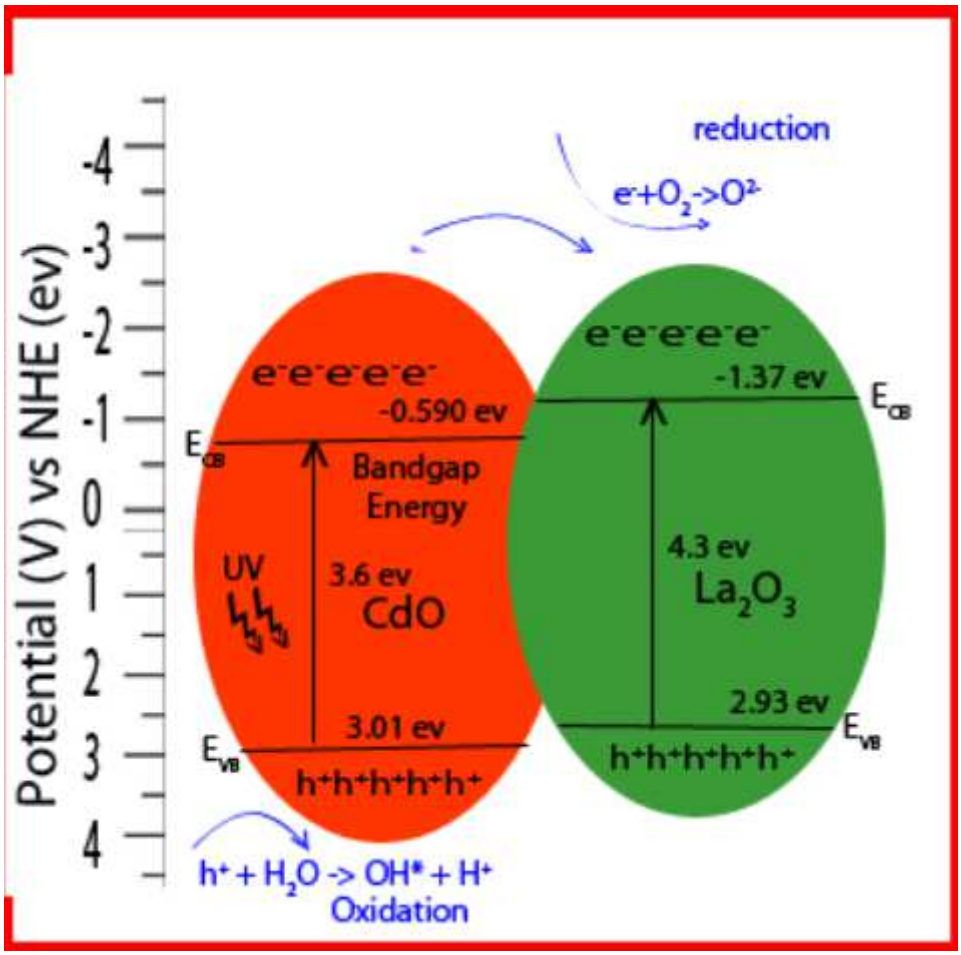

Figure 16

The schematic representation of photocatalytic mechanism of CdO, CdO/La2O3 and CdO/La2O3/PVP nanocomposite